# Surface Wave Modelling in the Wadden Sea

## Diploma Thesis

Alger Werft

Institut für Chemie und Biologie des Meeres
der
Carl-von-Ossietzky Universität Oldenburg

Diplom-Studiengang Marine Umweltwissenschaften

# Contents

# List of Figures

# List of Tables

# Chapter 1

# Introduction

On the grounds of the insight that waves are closely connected to the complete dynamics of coastal systems, a great interest is taken in the understanding of the major processes. Surface waves greatly affect the morphology by mobilizing sediment. Furthermore, they enhance fluxes of energy and momentum between the atmosphere and the ocean. Therefore, a detailed knowledge of waves is essential for the design of coastal projects since they are the major factor that determines the geometry of beaches, shore protection measures, offshore structures and other coastal works.

In this diploma thesis two models are introduced, a wave model called K-model which is based on the well known WAM (WAMDI, 1988), and the General Estuarine Transport Model (GETM), a circulation model especially developed for shallow water areas subjected to the influence of the tides. A one-sided coupling between GETM and the K-model has been implemented in such a way that current and sea surface elevation fields obtained with GETM are processed to input data for the wave model.

As an idealised application of the coupled model the influence of the currents on surface waves is studied. Simulations have been carried out to evaluate the impact of time varying current velocity fields on surface gravity waves. In addition, in this thesis different wind scenarios are examined with regard to the modulation of surface wave parameters like the significant wave height and the mean period.

This thesis is structured as follows: In the first chapter, the basic theory of spectral wave modelling is laid out and terms are explained. In the second and third chapter the wave and current models used for this thesis are introduced. The fourth chapter covers the model setup. Firstly, an explanation is given how the wave model has been coupled with the current model. Then the model domain and model forcing are described. In this context wave scenarios are presented to which the coupled model has been applied. The fifth chapter is concerned with the results of the case studies based on the wind scenarios followed by a discussion of these in the next chapter. Finally some conclusions are given.

## 1.1   Notation

Here, a few remarks on the notation used in the text are made.

Vectors are denoted in bold face. The three-dimensional space vector is given by $\boldsymbol{x}$ or as components by $(x, y, z)$, the three-dimensional velocity vector by $\boldsymbol{u}$ or $\boldsymbol{v}$ or as components by $(v, w, z)$, and the two-dimensional wave number vector by $\boldsymbol{k}$ or as components by $(k_x, k_y)$. The scalar product of vectors is indicated by a central dot. $t$ denotes time. Differentiation with respect to the space vector is indicated by $\nabla_{\boldsymbol{x}}$, and with respect to the wavenumber vector by $\nabla_{\boldsymbol{k}}$. Partial derivatives are given by $\partial$, e.g. $\partial_t$ with respect to time t or $\partial_y$ with respect to the spatial coordinate $y$. $\partial_{xx}$ stands for $\partial_x \partial_x$.
If an equation is refered to in the text, its number is given in parentheses.

# Chapter 2

# Theory of Spectral Wave Modelling

In this section the basic theory of spectral wave modelling is summarized. It is based on the summary given by Schneggenburger (1998a) and has been extendend by some of the theory given in Komen et al. (1994) where a complex derivation of the theory can be looked up. The following concepts are given in order to introduce terminology and formulae used in this work.

In general, spectral wave models predict the evolution of the sea state in a certain area. This prediction depends on the initial sea state, on boundary conditions and on external fields like wind, currents, and water depths. The objective is to describe the sea state on space and time scales which are large compared to typical wave lengths and wave periods. Hence the detailed evolution of the sea surface in time and space is not resolved.

The mathematical means of describing the state of the sea surface is the wave spectrum. A central role plays the wave action balance equation which gives the dynamics of wave spectra on large space and time scales. This equation is solved numerically by spectral wave models.

In the following, definitions of the wave spectrum are given. Additionally, the wave action balance equation is introduced. At the end of this chapter, integrated parameters of the spectrum are presented.

## 2.1 The Wave Spectrum

There are two different ways of defining wave spectra.

1. Either one with linear wave theory and uses an expression for the energy to define the wave spectrum afterwards, or,

2. firstly, the statistical theory of linear random waves is regarded, and then the wave number spectrum is defined by the Fourier transform of the two-point covariance function.

If the sea state is quasi-stationary and quasi-homogeneous, these two approaches will be equivalent and can be approximated by a superposition of slowly varying linear waves.

### 2.1.1 Linear Wave Theory and the Wave Spectrum

#### 2.1.1.1 The Linearised Equations of Motion and their Solutions

Our system of interest is composed of two fluids, air and water. Its dynamics are sufficiently described by the Navier-Stokes equation for a two-layer fluid. To reduce the complexity of this equation we consider the linearized Navier-Stokes equation for one-layer fluids in a gravitational field. This can be done because the density of air is much smaller than the density of water. The linearized Navier-Stokes equation describes waves in good approximation.

Further approximations can be made. Ocean waves can be considered to be free. Therefore forcing by the environment can be neglected. With regard to longer waves (with wavelengths $\lambda > 1\,\mathrm{m}$) viscosity and surface tension can also be ignored. Furthermore, the Coriolis force is not taken into account because of the inverse Coriolis parameter being much larger than a typical wave period. With these assumptions, the Navier-Stokes equation reduces to the Euler equation for a one-layer fluid.

Moreover, water is hard to compress, and for our purpose, we will assume water to be incompressible. In an incompressible fluid, the velocity $\boldsymbol{v} =$

$(u, v, w)$ at each point will satisfy the equation of continuity

$$\partial_x u \,+\, \partial_y v \,+\, \partial_z w \,=\, 0. \tag{2.1}$$

In additon, given the irrotationality of the surface wave motion (Komen et al., 1994), gravity waves on the surface can be descibed by a velocity potential $\phi(\boldsymbol{x}, z, t)$ for the wave flow field with the property

$$u \,=\, \partial_x \phi, \;\; v \,=\, \partial_y \phi, \;\; w \,=\, \partial_z \phi \tag{2.2}$$

and a surface elevation field $\eta(\boldsymbol{x}, t)$. $\eta$ gives the deviation of the water-air boundary from its mean (equilibrium) value. The vector $\boldsymbol{x}$ has two components $(x,y)$, the horizontal location coordinates, $z$ denotes the vertical space coordinate.

According to these assumptions one may introduce the velocity potential in the continuity equation (2.1)

$$\partial_{xx} \phi \,+\, \partial_{yy} \phi \,+\, \partial_{zz} \phi \,=\, 0, \;\; z < \eta(x, y, t) \tag{2.3}$$

resulting in Laplace's equation.

On the free water surface boundary, this equation is specified by the kinematic and the dynamical boundary conditions.

The physical condition that a fluid particle at the surface should remain there at all times is called the kinematic boundary condition, given by

$$\partial_t \eta \,+\, \partial_x \phi \partial_x \eta \,+\, \partial_y \phi \partial_y \eta \,=\, \partial_z \phi, \;\; z = \eta(x, y, t)\,. \tag{2.4}$$

The other condition to be satisfied at the surface is based upon the fact that the pressure at the surface must be equal to the atmospheric pressure. This boundary condition makes use of Bernoulli's relation. With regard to the simplification to a one-layer fluid, the pressure is zero in the vaccum just above the sea surface. Therefore, it should be zero just below the sea surface. This condition, dealing with the force on the surface, is usually called the dynamic boundary condition, given by

$$\partial_t \phi \,+\, \frac{1}{2} \left[ (\partial_x \phi)^2 \,+\, (\partial_y \phi)^2 \right] \,+\, g\,\eta \,=\, 0, \;\; z = \eta(x, y, t)\,. \tag{2.5}$$

In (2.5), $g$ is the gravitational acceleration.

Since the nonlinear equations cannot be solved, they are simplified by linearisation, that is by expanding arguments depending on $\eta$ and by retaining only terms linear in the wave steepness. This wave steepness, considered to be a small parameter, can be defined in a general way by assuming that $\eta$ is characterised by both a vertical and a horizontal length scale, in such a way that their ratio is small. This ratio is then taken as the expansion parameter $\epsilon = kh$. To obtain the linearised equations one makes formal expansion around $\epsilon = 0$ (Phillips, 1977).

The potential flow equations then read

$$\partial_{xx}\phi \,+\, \partial_{yy}\phi \,+\, \partial_{zz}\phi \;=\; 0, \;\; z < 0 \tag{2.6}$$

$$\left.\begin{array}{rcl} \partial_t\eta &=& \partial_z\phi, \\[2mm] \partial_t\phi \,+\, g\,\eta &=& 0, \end{array}\right\} z = 0. \tag{2.7}$$

Only for waves with infinitisemal amplitudes the linearised equations yield exact solutions. If the solutions of the nonlinear equations are developed as a power series in terms of $\epsilon$ (Stokes expansion), it can be seen that the solutions of the linearized equations are equal to the first terms of this expansion (Whitham, 1974). In spectral wave modelling only the linear solutions are considered.

The solutions of the linearized system can be given as normal mode solutions for the surface elevation field $\eta$ and the velocity potential $\phi$. In the solutions the wavenumber vektor $\boldsymbol{k}$ occurs. The wave number in direction of $x$ is given by $k_x = 2\pi/\lambda_x$ where $\lambda_x$ is the wavelength, defined in (2.13), in direction of $x$. $k_y$ is defined analogously. For each $\boldsymbol{k}$, two solutions ($\pm$) exist

$$\eta(\boldsymbol{x},t) \;=\; a\,\exp\left[i\left(\boldsymbol{k}\cdot\boldsymbol{x} \,-\, \omega_\pm\,t\right)\right] \,+\, c.c. \tag{2.8}$$

$$\phi(\boldsymbol{x},z,t) \;=\; -i\omega_\pm\,a\,\frac{\exp(kz)}{k}\,\exp(i\left(\boldsymbol{k}\cdot\boldsymbol{x} \,-\, \omega_\pm\,t\right)) \,+\, c.c.$$

where c.c. denotes the complex conjugate of the right-hand side term, and $k$ the modulus of the wavenumber vector $\boldsymbol{k}$.

In shallow water with a flat bottom at depth $z = -h$ the boundary conditions at the bottom are

$$\partial_z\phi \;=\; 0, \;\; z = \text{-h}. \tag{2.9}$$

The solutions of the linearized equations (2.8) become

$$\eta(\boldsymbol{x}, t) \;=\; a \, \exp\left[i\left(\boldsymbol{k} \cdot \boldsymbol{x} - \omega_\pm \, t\right)\right] \;+\; c.c. \tag{2.10}$$

$$\phi(\boldsymbol{x}, z, t) \;=\; -\, i\omega_\pm \, a \, \frac{\cosh\left[k\left(z + h\right)\right]}{k \, \sinh kh} \, \exp\left[i\left(\boldsymbol{k} \cdot \boldsymbol{x} - \omega_\pm \, t\right)\right] \;+\; c.c.$$

with the circular frequencies

$$\omega_\pm \;=\; \pm\sigma(\boldsymbol{k}) \;+\; \boldsymbol{k} \cdot \boldsymbol{u}_c \tag{2.11}$$

and the dispersion relation

$$\sigma^2(\boldsymbol{k}) \;=\; gk \, \tanh kh. \tag{2.12}$$

The second term on the right-hand side of (2.11) is the Doppler shift due to the current with the velocity $\boldsymbol{u}_c$. The dispersion relation giving the relationship between the wavenumber vector and the circular frequency implies that the wave period depends not only on the wavelength, defined in (2.13), but also on the water depth.

The normal mode solutions (2.8) relate to plane waves represented by the phase $\Theta$ and the amplitude $a$. The phase of the waves is $\Theta = (\boldsymbol{k} \cdot \boldsymbol{x} - \omega_\pm t)$. It varies between 0 and $2\pi$. The amplitude $a$ of plane waves is complex. The wavelength $\lambda$ is the horizontal distance between two identical points on two successive wave crests or two successive wave troughs. The time interval between the passage of two successive wave crests or troughs at a given point is the wave period $T$.

The wavelength $\lambda$ and wave period $T$ are defined as

$$\lambda \;=\; \frac{2\pi}{k}, \; T \;=\; \frac{2\pi}{\omega_+}. \tag{2.13}$$

In shallow water, the general solution of $\eta$ is obtained by a superposition of the normal mode solutions from (2.10). This superposition corresponds to a Fourier representation of the sea surface with the solution for $\eta$ in (2.10) giving a Fourier mode. Since the surface elevation is real, the $\omega_-$ mode can be replaced by the complex conjugate of the $\omega_+$ mode. The general solution symplifies to

$$\eta(\boldsymbol{x}, t) \;=\; \int_{-\infty}^{\infty} a(\boldsymbol{k}) \, \exp[i(\boldsymbol{k} \cdot \boldsymbol{x} - \omega t)] \, d\boldsymbol{k} \;+\; c.c. \tag{2.14}$$

where the subscript $+$ of $\omega$ has been dropped.

### 2.1.1.2   The Wave Spectrum

The expression for the energy density of waves will now be introduced which leads directly to the definition of the wave spectrum. The energy contained in waves is described by the energy density per unit horizontal area of the sea surface. Its unit is $\mathrm{Jm}^{-2}$. A wave has potential energy because water parcels move up and down in the gravity field. It also has kinetic energy associated with the velocities of the water parcels. To obtain the energy density the sum of the potential and the kinetic energy per unit volume is integrated with respect to the vertical coordinate $z$.

$$\mathcal{E} \;=\; \frac{1}{2}\rho g\,\eta^2 \;+\; \frac{1}{2}\,\rho \int_{-\infty}^{\eta} \left[ (\partial_x \phi)^2 \;+\; (\partial_y \phi)^2 \;+\; (\partial_z \phi)^2 \right]\, dz \qquad (2.15)$$

$\rho$ denotes the density of water and $g$ the gravitational acceleration.

The first term is the potential energy density, and the second the kinematic energy density, which is expressed in terms of the velocity potential.
Note, that the total energy is given by

$$E_{tot} \;=\; \int\!\int \mathcal{E}\, dxdy. \qquad (2.16)$$

If one wants to consider only waves in a limited area given by the total surface $A$, an expression of the energy density per unit area with regard to the region under consideration is derived by

$$\bar{\mathcal{E}} \;=\; \frac{1}{A}\int\!\int \mathcal{E}\, dxdy. \qquad (2.17)$$

The spatially mean energy per unit area of a normal mode is then derived by substituting (2.8) in (2.17) with the result

$$\bar{\mathcal{E}} \;=\; 2\,\rho\,g\,|a|^2. \qquad (2.18)$$

$|\cdot|$ defines the modulus.

Using the Fourier representation in equation (2.14), an expression for the spatial average energy per unit area of the wave field described by the superposition of normal modes is obtained as

$$\bar{\mathcal{E}} \;=\; 2\rho g \int |a(\boldsymbol{k})|^2 \, d\boldsymbol{k} \,. \tag{2.19}$$

Considering an ensemble of several possible representations of the surface elevation field in a given situation, a specification of $\bar{\mathcal{E}}$ is derived by giving the ensemble mean energy density. The wave energy spectral density or simply the wave spectrum $F$ used in spectral wave models is then defined by this ensemble average energy density $\langle \bar{\mathcal{E}} \rangle$

$$\langle \bar{\mathcal{E}} \rangle \;=\; \rho g \int F(\boldsymbol{k}) \, d\boldsymbol{k} \tag{2.20}$$

as

$$F(\boldsymbol{k}) \;=\; 2 \langle |a(\boldsymbol{k})|^2 \rangle \,. \tag{2.21}$$

Here, $\langle ... \rangle$ denotes the ensemble average.

The wave (energy) spectrum $F(\boldsymbol{k})$ is of central importance in the description of ocean waves. It specifies the energy content of waves characterised by $\boldsymbol{k}$. Therefore, we know which waves contain the most energy and are subsequently dominating the wave field.


## 2.1.2   Statistical Theory of Linear Random Waves

In practice it is impossible to specify the initial sea state completely because the Fourier modes cannot be determined with the correct phases. With a statistical description of the sea surface this obstacle can be overcome.


The probability of finding a particular sea state with $\eta(\boldsymbol{x}, t)$ as a field of random waves is now considered. Like in the previous section $\eta(\boldsymbol{x}, t)$ describes the deviation of the sea surface from its mean level at different locations and times. In order to get an image of a random wave field one regards the surface elevation $\eta_i$ at a point $(\boldsymbol{x}_i, t_i)$ as a random variable. Thus, $\eta_i$ has a certain probability distribution. The following statistical concepts are presented as found in Bauer (1991).

The joint probability distribution function of the random variables $\eta_1, ..., \eta_n$

$$W_{\eta_1, \eta_2, ..., \eta_n}(\xi_1, ..., \xi_n) \; = \; P(\eta_1 \leq \xi_1, \eta_2 \leq \xi_2, ..., \eta_n \leq \xi_n) \qquad (2.22)$$

gives the probability that the surface displacements $\eta_i$, $i = 1, ..., n$, at the points $(\boldsymbol{x}_i, t_i)$ have values below $\xi_i$ . $P$ is some probability messure.

If the joint probability density $w_{\eta_1, ..., \eta_n}$ of equation (2.22) is known, the moments can be computed, e.g. the first moment as

$$\langle \eta(\boldsymbol{x}_1, t_1) \rangle \; = \; \int_{-\infty}^{+\infty} \xi_1 w_{\eta_1}(\xi_1) \, d\xi_1 \qquad (2.23)$$

and the second moment as

$$\langle \eta(\boldsymbol{x}_1, t_1)\eta(\boldsymbol{x}_2, t_2) \rangle \; = \; \int_{-\infty}^{+\infty} \int_{-\infty}^{+\infty} \xi_1 \xi_2 w_{\eta_1, \eta_2}(\xi_1, \xi_2) \, d\xi_1 d\xi_2 \, . \qquad (2.24)$$

The probability density of the random variable $\eta_1$ and the joint probability density of the random variables $\eta_1$ and $\eta_2$ are given by

$$w_{\eta_1}(\xi_1) \; = \; \int_{-\infty}^{+\infty} \cdots \int_{-\infty}^{+\infty} w_{\eta_1, ..., \eta_n}(\xi_1, ..., \xi_n) d\xi_2 ... d\xi_n \qquad (2.25)$$

$$w_{\eta_1, \eta_2}(\xi_1, \xi_2) \; = \; \int_{-\infty}^{+\infty} \cdots \int_{-\infty}^{+\infty} w_{\eta_1, ..., \eta_n}(\xi_1, ..., \xi_n) d\xi_3 ... d\xi_n \, .$$

Note, that the density $w_{\eta_1}$ has the unit $\mathrm{m}^{-1}$, and the joint density $w_{\eta_1, \eta_2}$ the unit $\mathrm{m}^{-2}$.

To be able to compute the moments of this random surface one has to make the assumption that the surface is Gaussian. Then the probability density $w_{\eta_1, ..., \eta_n}$ is known and the integrals of the equations (2.23) and (2.24) can be evaluated. This is not an arbitrary assumption due to the fact that real ocean surfaces have turned out to be very closely Gaussian (Komen et al., 1994). There are slight deviations, the most notable is that the wave crests are a little higher than the wave troughs are low. This gives the surface a certain asymmetry which is not reflected in the normal distribution.

Since the distribution is Gaussian the statistical information is basically contained in the first two moments. But as $\eta(\boldsymbol{x}, t)$ describes the deviation of the sea surface from its mean level, the first moment $\langle \eta(\boldsymbol{x}, t) \rangle$ is zero.

Therefore, the statistical information for the $\eta$ field is entirely given by the second moment, the two-point covariance function $\mathcal{F} = \langle \eta(\boldsymbol{x}_1, t_1) \eta(\boldsymbol{x}_2, t_2) \rangle$.

Assuming statistical stationarity and homogeneity, which can be defined as the invariance of all ensemble averages under space and time translations $x \rightarrow x' = x + \xi$, $t \rightarrow t' = t + \tau$, the two-point covariance function $\mathcal{F}$ only depends on the difference of locations $\boldsymbol{\xi}$ and difference of times $\tau$ and is independent of $\boldsymbol{x}$ and $t$

$$\mathcal{F}(\boldsymbol{\xi}, \tau) = \langle \eta(\boldsymbol{x} + \boldsymbol{\xi}, t + \tau) \, \eta(\boldsymbol{x}, t) \rangle. \tag{2.26}$$

One can define the wave spectrum by determining the three-dimensional Fourier transform $F(\boldsymbol{k}, \omega)$ of the covariance function $\mathcal{F}$ with respect to $\boldsymbol{\xi}$ and $\tau$. Integrating the Fourier transform $F(\boldsymbol{k}, \omega)$ over the positive frequencies $\omega$ one obtains the wave spectrum

$$F(\boldsymbol{k}) \equiv \int_0^\infty F(\boldsymbol{k}, \omega) \, d\omega \,. \tag{2.27}$$

With the help of the dispersion relation and (2.14) taken to be valid for $\eta$ in (2.26), the dynamics of the sea surface can be reintroduced. Then (2.21) and (2.27) as definitions of $F(\boldsymbol{k})$ are equivalent (Komen et al., 1994).

## 2.2 Extension to Inhomogeneous Systems

In the previous section free, linearized water wave equations were analysed. Now an analysis of more general situations is given. A generalisation of (2.8) is considered in which the amplitude, the frequency and the wavelength are allowed to vary slowly. An example of such a situation is swell on currents varying slowly in space and time in a shallow sea whose bottom depth also varies slowly.

If waves are allowed to change slowly with time and space, equation (2.8) becomes

$$\eta(\boldsymbol{x}, t) = a(\boldsymbol{x}, t) \, \exp(i \, \theta(\boldsymbol{x}, t)), \tag{2.28}$$

where both the amplitude $a(\boldsymbol{x}, t)$ and the phase function $\Theta(\boldsymbol{x}, t)$ vary slowly with $\boldsymbol{x}$ and $t$. The phase function is given by

$$\Theta(\boldsymbol{x}, t) \;=\; \Theta(0,0) \,+\, \boldsymbol{x} \cdot \nabla_{\boldsymbol{x}}\Theta \,+\, t\partial_t\Theta \tag{2.29}$$

where $\Theta(0, 0)$ is the initial phase.

Equation (2.28) describes so called wave trains. A wave train is a regional wave created by a superposition of an infinite number of waves having different phases and amplitudes.

The wavenumber vector and the local circular frequency of wave trains can be defined with the help of derivatives of the phase function

$$\boldsymbol{k}(\boldsymbol{x}, t) \;=\; \nabla_{\boldsymbol{x}}\Theta(\boldsymbol{x}, t), \tag{2.30}$$

$$\omega(\boldsymbol{x}, t) \;=\; -\partial_t\Theta(\boldsymbol{x}, t). \tag{2.31}$$

The dispersion function $\Omega$ defines the dispersion relation between the circular frequency and the wave vector. For linear gravity wave trains it is given by

$$\omega(\boldsymbol{x}, t) \;=\; \Omega[\boldsymbol{k}(\boldsymbol{x}, t), \boldsymbol{u}_c] \;=\; \sigma[\boldsymbol{k}(\boldsymbol{x}, t), h(\boldsymbol{x})] \,+\, \boldsymbol{k}(\boldsymbol{x}, t) \cdot \boldsymbol{u}_c \tag{2.32}$$

with the current $\boldsymbol{u}_c(\boldsymbol{x}, t)$ and the depth $h(\boldsymbol{x})$.

In slowly varying media the local intrinsic frequency $\sigma$ as defined in (2.12) becomes

$$\sigma(\boldsymbol{k}(\boldsymbol{x}, t), \boldsymbol{x}, t)^2 \;=\; gk(\boldsymbol{x}, t)\,\tanh[k(\boldsymbol{x}, t)h(\boldsymbol{x})]. \tag{2.33}$$

When confusion is unlikely, we will drop the arguments $\boldsymbol{x}$ and $t$.

## 2.3   The Wave Action Balance Equation

We now introduce the wave action balance equation giving the dynamics of wave spectra. This equation is solved numerically by spectral wave models.

If depth and currents are varying, i.e. in the case of an inhomogeneous medium, the following equation gives the time evolution of the amplitude $a$ of the wave trains

$$\partial_t N + \nabla_{\boldsymbol{x}}(\nabla_{\boldsymbol{k}}\Omega\, N) = \partial_t N + \nabla_{\boldsymbol{x}}(\boldsymbol{v}_D N) = 0 \qquad (2.34)$$

with

$$N(\boldsymbol{x}, t) = \frac{2|a(\boldsymbol{x}, t)|^2}{\sigma}. \qquad (2.35)$$

$N$ is called the action density of a wave train.

The group velocity $\boldsymbol{v}_D$ of a wave train is defined by $\nabla_{\boldsymbol{k}}\Omega$. It is the sum of the intrinsic wave group velocity $\boldsymbol{c}_g = \nabla_{\boldsymbol{k}}\sigma$ and the current velocity $\boldsymbol{u}_c$

$$\boldsymbol{v}_D = \nabla_{\boldsymbol{k}}\Omega = \nabla_{\boldsymbol{k}}\sigma(\boldsymbol{k}) + \boldsymbol{u}_c = \boldsymbol{c}_g + \boldsymbol{u}_c. \qquad (2.36)$$

$\boldsymbol{v}_D$ is the velocity with which the energy of the wave train propagates.

Note that equation (2.34) has the general form of a conservation law. The local rate of change of a density is determined by a flux of that density. The detailed derivaton of (2.34) will not be given here. It can be found in Bretherton and Garrett (1968).

Equation (2.14) gives a generalized solution for the linearized water waves in homogeneous environmental conditions. To account for perturbations, we considered wave trains in order to give a better approximation of reality. But as the sea surface is not realistically described by one wave train (2.28), we use a superposition of wave trains. Its spatially mean energy density is

$$\bar{\mathcal{E}} = 2\rho g \int |a(\boldsymbol{k}, \boldsymbol{x}, t)|^2 \, d\boldsymbol{k}. \qquad (2.37)$$

$\bar{\mathcal{E}}$ is now a function of $\boldsymbol{x}$ and $t$ on the slow space and time scale.

The definition of the wave spectrum in (2.21) generalizes to

$$F(\boldsymbol{k}, \boldsymbol{x}, t) = 2\langle |a(\boldsymbol{k}, \boldsymbol{x}, t)|^2 \rangle. \qquad (2.38)$$

Willebrand (1975) noted that the conservation of wave action expressed in (2.34) holds for every wave component separately, so that a spectral wave action density (depending on $\boldsymbol{k}$) can be considered

$$N(\boldsymbol{k}, \boldsymbol{x}, t) = \frac{F(\boldsymbol{k}, \boldsymbol{x}, t)}{\sigma} = \frac{2\langle |a(\boldsymbol{k}, \boldsymbol{x}, t)|^2 \rangle}{\sigma}. \qquad (2.39)$$

The resultant wave action balance equation is

$$\partial_t N + \nabla_{\boldsymbol{x}} \cdot (\dot{\boldsymbol{x}} N) + \nabla_{\boldsymbol{k}} \cdot (\dot{\boldsymbol{k}} N) = 0. \tag{2.40}$$

The 'dot terms' $\dot{\boldsymbol{x}}$ and $\dot{\boldsymbol{k}}$ in (2.40) are determined by

$$\dot{\boldsymbol{x}} = \nabla_k \Omega \tag{2.41}$$

$$\dot{\boldsymbol{k}} = -\nabla_{\boldsymbol{x}} \Omega. \tag{2.42}$$

Equation (2.40) is a generalisation of (2.34). It implies that the total wave action defined by

$$A_{tot} = \rho g \int \int N(\boldsymbol{k}, \boldsymbol{x}, t)\, d\boldsymbol{x} d\boldsymbol{k} \tag{2.43}$$

is conserved. In deep water and without currents, equation (2.40) reduces to the simpler form

$$\partial_t F + \nabla_{\boldsymbol{x}} \cdot (\boldsymbol{c}_g\, F) = 0. \tag{2.44}$$

As the wave spectrum is closely related to the energy density $\mathcal{E}$ (see equation (2.20)), (2.44) expresses the conservation of energy. As stated above, the group velocity $\boldsymbol{v}_D$ can be interpreted as the propagation velocity of energy. The total energy in an area only changes because of energy flowing in and out through the boundaries. Energy conservation only holds in the absence of currents and energy changing processes. Generally speaking, the total energy content in an area may change because waves may lose or gain energy as a result of interaction with currents. For this reason, equation (2.40) is the more general conservation law expressing the conservation of wave action.

## 2.4 Integrated Parameters of the Spectrum

Related to the wave spectrum is a series of characteristic numbers called the spectral moments. These are integrated parameters of the wave spectrum which can be indentified with observed parameters of the sea state. Consequently, it is possible to compare wave model results with measurements.

The moments of a spectrum are defined by

$$m_n \; = \; \int F(f,\theta) f^n \, df \, d\theta, \;\; n = 0,1,2... \; . \tag{2.45}$$

$F(f,\theta)$ is the frequency-directional spectrum exlained in appendix (see A.2). The spectral moment $m_0$ represents the total energy or the variance of the surface. The square root of the variance of the sea surface is its standard deviation. The standard deviation is a common measure for the variations about the mean and is thus a reasonable scale for the surface height variations. Therefore, the moment $m_0$ can be used to give a definition of the significant wave height $H_s$

$$H_s \; \equiv \; 3.8\sqrt{m_o} \; \approx \; 4.0\sqrt{m_o}. \tag{2.46}$$

$H_s$ is related to the observable significant wave height $H_{1/3}$ which gives the height of the highest $1/3$ of oberved waves. It is traditionally estimated by means of visual observation of the sea state.

Based on the moments of the spectrum different integrated periods can also be derived as

$$\langle T \rangle \; \equiv \; \frac{m_{-1}}{m_0}, \;\; T_{m1} \; \equiv \; \frac{m_0}{m_1}, \;\; T_{m2} \; \equiv \; \sqrt{\frac{m_0}{m_2}} \, . \tag{2.47}$$

Here, $\langle T \rangle$ is the mean period of the waves. The period $T_{m2}$ can be indentified as the zero-crossing period $T_z$ derived from observations. The zero-crossing technique is applied to an irregular wave record. According to this technique, a wave is defined when the surface elevation crosses the zero-line, i.e. the mean water level, either upwards or downwards, and continues until the next crossing point in the same direction. The period of waves defined this way is the zero-crossing period $T_z$ (Demirbilek et al., 2002).

The mean direction of the wave vector giving the mean wave direction is defined as

$$\langle \theta \rangle \; \equiv \; \arctan\left( \frac{\int F(f,\theta)\, \sin\theta \, df \, d\theta}{\int F(f,\theta)\, \cos\theta \, df \, d\theta} \right). \tag{2.48}$$

An explanation for the term peak frequency $f_p$ is added here. It is not an integrated parameter of the spectrum. But it is often used to discuss the

form of spectra. The peak frequency is the frequency for which the $F(f)$ attains its maximum

$$F(f_p) \ = \ \max_f F(f) \tag{2.49}$$

where $F(f)$ is the frequency spectrum defined in appendix (A.3).

# Chapter 3

# Description of the Wave Model

## 3.1   The Wave Action Balance Equation

The K-model is a spectral discrete wave model. It numerically solves the wave action balance equation (2.40) in a generalised version. In order to more completely describe the processes of wave generation sources and sinks of wave action have to be taken into account. These terms are introduced in the balance equation on the right-hand side as $S(N)$.

Equation (3.1) is solved in $\boldsymbol{k}$-space using the polar coordinates $(k, \theta)$. $k$ is the modulus of the wavenumber vector, and $\theta$ the direction of the wavenumber vector.

In these coordinates the wave action balance equation is given by

$$\partial_t N \ + \ \partial_{\boldsymbol{x}} \cdot (\dot{\boldsymbol{x}} N) \ + \ \partial_k \cdot (\dot{k} N) \ + \ \partial_\theta \cdot (\dot{\theta} N) \ = \ S(N). \tag{3.1}$$

It describes the evolution of the wave action density $N$ for a wave field consisting of a superposition of slowly varying inhomogeneous wave trains (cf. section 2.3).

The wave action density $N$ has been defined as $N = F/\sigma$ in (2.39), with $F$ and $\sigma$ as the spectral wave energy density and the wave intrinsic frequency, respectively. As stated before, $N$, $F$, and $\sigma$ are functions of the polar wave vector coordinates $(k, \theta)$, and of location $\boldsymbol{x}$ and time $t$. For brevity the arguments have been dropped in the notation.

The first term on the left-hand side of (3.1) describes the local rate of change of spectral wave action with time. The second term specifies the propagation in the $\boldsymbol{x}$-space including bottom- and current-induced straining. Bottom-induced straining is commonly known as shoaling. The third and fourth terms describe the redistribution of wave action density over the spectrum. In the wave number space (third term) it corresponds to a change of wave number due to straining of the wave field. In the direction space (fourth term) this corresponds to a change of direction of a spectral component known as refraction (Tolman, 1990).

The right-hand side of (3.1) represents the sum of external influences resulting in sources and sinks of wave action

$$S(N) = S_{in} + S_{phil} + S_{dis} + S_{bot}. \tag{3.2}$$

In the case of the K-model these influences consist of a modified Synder wind input $S_{in}$, a modified Phillips wind input $S_{phil}$, dissipation due to wave turbulence interactions $S_{dis}$, and dissipation by bottom interactions $S_{bot}$. The different source terms are explained below.

## 3.2   Source Functions

In the following, the individual source functions of the K-model are discussed. Firstly, a description is given of the source terms that represent the input of energy by the wind into the water. Secondly, dissipative processes involved in the wave generation are specified. At the end of this section, other possible source terms are shortly listed.

### 3.2.1   Energy Input by Wind

The wind input source terms represent the work done by the wind on the ocean surface to produce waves. The generation of waves by wind is commonly explained by Phillips' and Miles' mechanisms (Phillips, 1957, and Miles, 1957) which represent two successive physical processes during the generation of waves by wind. These two mechanisms and their resultant

source functions are described in the following.

The source functions used in the K-model are given here in terms of the friction velocity $u_*$. It is defined as the square root of the kinematic wind stress $\tau = C_D\, u_{10}^2$

$$u_* = \sqrt{C_D\, u_{10}^2}. \tag{3.3}$$

The friction velocity depends on the wind speed at a heigth of 10 m $u_{10}$, and on the drag coefficient $C_D$. In spectral wave modelling, the energy input by wind is commonly given in terms of $u_*$. In the K-model itself, the friction velocity $u_*$ is replaced by the wind speed in 10 m height using the fixed relation $28u_* \rightarrow 1.2u_{10}$.

### 3.2.1.1   Phillips Wind Input

The initial wave growth is due to turbulent pressure fluctuations in the air flow. As these fluctuations in the wind travel across the ocean, they generate small waves on the initially calm sea. Phillips (1957) showed that waves which travel at the same speed as the atmospheric pressure disturbances grow most rapidly through resonance with the advected pressure field. It should be noted that the resonant forcing does not occur continuously, because the atmospheric pressure pattern is turbulent. The resonance rather takes place in a random series of short impulses (LeBlond & Mysak, 1978). Wave growth during this phase depends only on the wind speed and is independent of the wave height, and hence of the wave spectrum. Therefore, Phillips' mechanism results in a growth of waves linear in time given by

$$\partial_t N \;=\; S_{phil} \;=\; \alpha, \tag{3.4}$$

where the constant $\alpha$ quantifies the amount of energy transferred from the wind to the sea. $\alpha$ is also called Phillips' parameter.

In the K-model, the version of the Phillips input source function described by Cavaleri et al. (1981) is used. Two extensions were added to this source function.
The filter of Tolman (1992) prevents an increase of energy for frequencies less

than the Pierson-Moskowitz frequency $f_{PM}$ (Pierson et al., 1964, cf. section A.4.1).

To include a decreasing energy input for increasing frequencies, another filter was added by Schneggenburger et al. (1998). This accounts for the effect described by Phillips (1977). He stated that energy input due to atmospheric pressure disturbances only occurs for waves that approximately obey the relation $u_{10}/c < 1.5$.

The modified Phillips input is given by

$$
S_{phil} = 0.1 \cdot 2 \frac{80\rho_a^2}{g^2 \rho_w^2} \frac{c_g}{\sigma} \left[ u_* \cos(\theta - \theta_{\mathrm{w}}) \right]^4 \tag{3.5}
$$

$$
\cdot \underbrace{\exp\left[ -\left( \frac{f}{f_{PM}} \right)^{-4} \right]}_{Tolman\,filter} \underbrace{\exp\left[ -\left( \frac{f}{f_{PM}} \right) \right]}_{Schneggenburger\,filter} ,
$$

where $\theta - \theta_{\mathrm{w}}$ is the relative angle of the wind direction $\theta_{\mathrm{w}}$ and the wave vector direction $\theta$. $\rho_a$ and $\rho_w$ are the densities of air and water, respectively.

This source function is needed to allow for a model startup from initial conditions of a completely calm sea, i.e. initially no energy is contained in the wave field. Furthermore, it is necessary after periods of zero winds, so that the wave energy can recover (Schneggenburger et al., 1998b). It is especially important in small scale applications to enclosed systems because in such cases the propagation of swell into the model area is hampered and it is unlikely to find residual swell after calm periods.

The source function was lowered to one-tenth of its original magnitude in order to reduce the input for short waves in small-scale applications. Otherwise this source function would contribute too much energy to the spectra.

### 3.2.1.2 Snyder Wind Input

After a period of initial wave growth the waves are of sufficient height so that they interfere with the wind flow across the sea surface. This leads to the generation of regions of high and low pressure on either side of the crests. These pressure gradients reinforce the process of wave growth. The

waves now grow more rapidly, i.e. exponentially, due to this feedback process (Miles, 1957).

The exponential growth of the wave action is given by

$$\partial_t N \;=\; S_{in} \;=\; \beta N, \tag{3.6}$$

where the constant $\beta$ controls the energy input to the sea.

The growth parameter $\beta$ is used in wave models in a parametric form. Snyder et al. (1981) carried out measurements of the growth parameter $\beta$ and proposed the following empirical fit.

$$\beta \;=\; \beta_0 \,\omega \max \left[ 28 \frac{u_*}{c} \cos(\theta - \theta_{\mathrm{w}}) - 1, \, 0 \right], \tag{3.7}$$

$$\beta_0 \;=\; 0.25 \frac{\rho_a}{\rho_w} \;\approx\; 0.0003.$$

In (3.7), $c$ denotes the phase velocity.

The Snyder wind input was used in WAM in a modified form (WAMDI, 1988). It was further altered by Schneggenburger et al. (1997) to take into account the effect of wind gustiness. This modification was adopted from Komen et al. (1994). They considered fluctuations in the wind field with a time scale longer than $1/\omega$, where $\omega$ is a typical frequency of the surface gravity waves. This part of the turbulent wind spectrum is called gustiness. To investigate the effect of gustiness on the wave growth, the friction velocity $u_*$ is assumed to be a Gaussian distributed stochastic variable with a steady and a fluctuating part, so that the growth parameter as well comprises a steady and a varying part. By taking the average, Komen et al. (1994) obtained the growth parameter $\beta = \beta_0 \,\omega\, G$.

Taking this into consideration, the modified Snyder source function is

$$S_{in} \;=\; \beta_0 \,\sigma\, G\, N(\boldsymbol{k}). \tag{3.8}$$

Note, that only the intrinsic frequency $\sigma$ is used and not the circular frequency $\omega$ given in (2.11). Schneggenburger (1998) argues that the effect of time varying currents on the source functions has not been sufficiently

quantified, and is therefore neglected.

For $\cos(\theta - \theta_w) > 0$, the gustiness parameter $G$ is given by

$$G = \frac{\sigma_{u*}}{\sqrt{2\pi}c_*} \exp\left[-\frac{(c_* - u_*)^2}{2\sigma_{u*}^2}\right] + \frac{1}{2}\left[\frac{u_*}{c_*} - 1\right]\left[1 - \Phi\left(\frac{c_* - u_*}{\sigma_{u*}}\right)\right]$$

(3.9)

with

$$c_* = \frac{\sigma}{28\,k\,\cos(\theta\,-\,\theta_{\mathrm{w}})}.$$

(3.10)

If $\cos(\theta - \theta_{\mathrm{w}}) \leq 0$, the gustiness parameter equals zero.

The function $\Phi$ in equation (3.9) is the probability distribution function of the standard normal distribution. It is given by

$$\Phi\left(x\right) = \frac{2}{\sqrt{2\pi}} \int_0^x \exp\left(-\frac{t^2}{2}\right) dt.$$

(3.11)

In (3.9), $\sigma_{u_*}$ denotes the standard deviation of the assumed Gaussian distribution for the friction velocity $u_*$.

The ratio of the standard deviation of the friction velocity to the friction velocity itself $\sigma_{u_*}/u_*$ describes the gustiness level. It is a tuning parameter of the K-model. In this work, it is chosen analogous to Schneggenburger (1998) as

$$\frac{\sigma_{u_*}}{u_*} = 0.4\,.$$

(3.12)

Figure (3.1) illustrates the growth rate for this gustiness level. In the case of normal dispersion, waves with a lower frequency travel faster than waves with a higher frequency. In order to get an understanding of the figure, take $u_*$ to be constant. Then the ratio $u_*/c$ is bigger for high-frequency waves and smaller for low-frequency waves. Therefore, the further left part of Figure (3.1) represents the growth of lower-frequency waves, and the further right part the growth of higher-frequency waves. From this, it can be concluded that gustiness has an impact on especially later stages of wave growth when low-frequency waves are dominant.
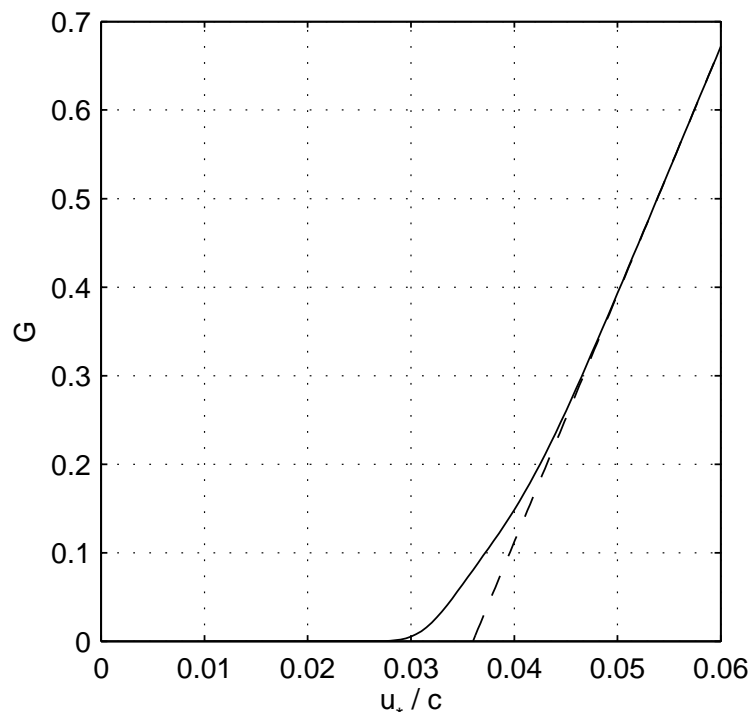
Figure 3.1: Growth rate for a gustiness level of $\sigma_{u_*}/u_* = 0.4$. The straight dashed line represents the wave growth in absence of wind gusts (Figure adapted from Komen et al., 1994).

## 3.2.2  Dissipation of Energy

Usually wave models take into account the dissipation of energy at the boundaries of the water body. On the one hand, energy is dissipated at the sea surface by whitecapping, and on the other hand, dissipation takes place at the bottom boundary, e.g. by bottom friction. As an alternative, Schneggenburger et al. (1997) incorporated the dissipation of wave energy due to interaction of the waves with turbulence into the K-model.

Below, a description is given of the source functions for dissipation by wave-bottom interactions and by wave-turbulence interactions.

### 3.2.2.1   Wave-Bottom Interactions

Next, we have to consider the bottom influence. In shallow water surface waves interact with the sea floor, because their orbital motion extends down to the bottom. Therefore, energy is dissipated at the bottom boundary. The interaction can occur in different ways, i.e. scattering, bottom friction, percolation, and bottom elasticity. What kind of interaction takes place depends on the bottom conditions. Scattering of wave components occurs on bottom irregularities, e.g. mesoscale sand ripples. Bottom friction increases with the height of the roughness elements on the sea bed. Percolation is enhanced by a high permeability of the bed material. If the bottom consists of mud, bottom elasticity plays a role. Scattering leads to a local redistribution of energy. The other three processes are dissipative. Shemdin et al. (1978) and Weber (1994) give an overview on this subject.

The bottom dissipation source function is not obtained by an interpretation of the physical mechanisms such as percolation or bottom friction. Instead, the bottom influence is represented on empirical grounds (Bouws & Komen, 1983) by

$$S_{bot} \; = \; -\Gamma\sigma^{-2}k^2(1 - \tanh^2 kh)N(\boldsymbol{k}) \tag{3.13}$$

where $\Gamma$ is the interaction coefficent. It is given by the chosen bottom interaction model (Komen et al. 1994).

Examples of bottom interaction models are the one-layer drag law by Hasselmann & Collins (1968) which relates the total bottom stress to the total velocity at a reference height, e.g. the top of the wave boundary layer, and the two layer eddy-viscosity model by Christoffersen & Jonsson (1985) in which the combined current-wave motion is split up into a wave component and a current component. Solving the boundary layer equation for the wave part yields a drag law for the wave bottom stress.

In the K-model, the interaction parameter is $\Gamma = 0.038 \, \mathrm{m^2 s^{-3}}$. This value is the JONSWAP result for swell dissipation (Hasselmann et al., 1973). Figure (3.2) depicts the bottom dissipation rate $-S_{bot}/N$ divided by the wave number $k$ as a function of nondimensional water depth $kh$ for the applied

interaction parameter. Keeping in mind the classification of surface gravity
waves as deep water waves with $kh \gg 1$ and shallow water waves with $kh \ll 1$,
it can be seen from Figure (3.2) that the bottom dissipation function affects
the waves as intended, i.e. shallow water waves are more exposed to bottom
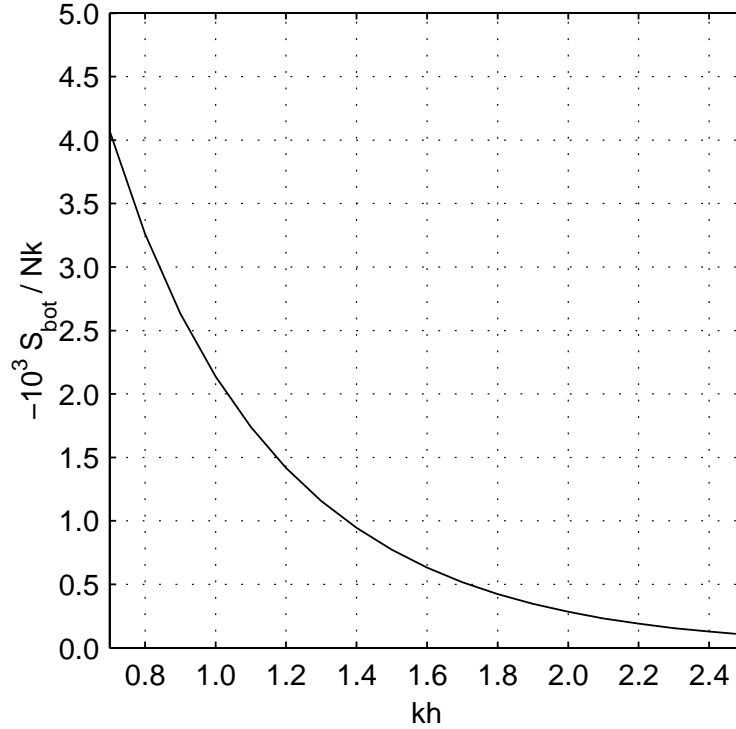dissipation.



Figure 3.2: The bottom dissipation rate $-S_{bot}/N$ divided by the
wavenumber $k$ as a function of nondimensional water depth $kh$ for
the interaction coefficient $\Gamma = 0.038 \, \mathrm{m^2 s^{-3}}$ (Figure adapted from
Komen et al., 1994).

Note, that the above source function has a general form. Theoretically,
equation (3.13) follows for either percolation or turbulent bottom friction
(Shemdin et al., 1978). Which mechanism actually dominates depends on
the sediment mean grain size.
In fact, Shemdin et al. (1978) have shown that the actual friction may vary
by as much as an order of magnitude, depending on the precise bottom con-
ditions. Since it is often difficult to fully describe the sediment conditions in
a model area, the different bottom interaction processes cannot be distin-
guished. Therefore, the above general form of the bottom source function is

used in wave modelling and an average interaction parameter is applied.

### 3.2.2.2 Wave-Turbulence Interactions

It is common in wave modelling to attribute the dissipation of wave energy at the surface boundary to whitecapping. Of all processes involved in the generation of surface gravity waves, dissipation by whitecapping is the last known. A spectral representation of the energy transfer rate associated with whitecapping is commonly given as a parameterization in the quasilinear form $S_{wc} = -\gamma_{wc}N$ with the interaction parameter $\gamma_{wc}$ being a functional of the wave spectrum (Hasselmann, 1974). The basic assumption of this parameterisation is that the white caps are preferentially situated on the forward face of the waves. Thereby, they exert a downward pressure on the upward moving water and hence do negative work on the wave (Donelan, 1994).

A different approach is to ascribe the dissipation of wave energy to the interaction of the waves with upper-oceanic turbulence (Schneggenburger, 1997). From such a point of view, wave breaking is not the only cause for a loss of wave energy. Other sources of turbulence are for example direct wind stirring, and negative buoyancy fluxes (Phillips, 1977).

Hence, the loss of wave energy is not solely due to whitecapping, but the general level of turbulence in the surface layer of the ocean has an impact on the waves.

The source function describing the wave turbulence interaction in the K-model was derived from turbulent diffusion in the hydrodynamic equations for the wave flow field (Rosenthal, 1989) as

$$S_{dis} \;=\; -\,\gamma\,g\,k^5\,\left(\coth 2kh + \frac{kh}{\sinh^2 kh}\right)\,N^2(\boldsymbol{k})\,. \tag{3.14}$$

The symbols $g$, $k$, and $h$ denote the gravitational acceleration, the modulus of the wave vector, and the local water depth, respectively. It is nonlinear to the order two in $N$.

The dissipation parameter $\gamma$ is given by

$$\gamma(N) \;=\; \gamma_0 \, \frac{p_1 \left(p_2 \frac{k}{\langle k \rangle}\right)^q + 1}{\left(p_2 \frac{k}{\langle k \rangle}\right)^q + 1} \;. \tag{3.15}$$

It is a function of the spectral mean wave number $\langle k \rangle$ which is determined from the spectral action density $N$. Hence, $\gamma$ is a functional of $N$. Since $\gamma$ depends on the mean wave number, a coupling between different action 'bins' is introduced in the model through $\gamma$.

The parameters $\gamma_0$, $p_1$, $p_2$, and $q$ determine the shape of $\gamma$. They were chosen in accordance with Schneggenburger et al. (2000) as

$$\gamma_0 \;=\; 0.09485, \;\; p_1 \;=\; 10.0, \;\; p_2 \;=\; 1.6, \; \text{and } q \;=\; 6.0. \tag{3.16}$$

In figure (3.3), the dissipation parameter $\gamma$ is displayed for this set of parameters. Its minimum and maximum are $\gamma_0$ and $p_1\gamma_0$, respectively. The parameter $p_2$ determines where $\gamma$ ascends relative to the mean wave number $\langle k \rangle$. The steepness of $\gamma$ in $k$ is regulated by $p_2$ and $q$.

Since $\gamma(N)$ increases with $k/\langle k \rangle$, it parameterises the more intense dissipation of short waves in a wave spectrum (Schneggenburger et al., 2000).

### 3.2.3   Other Source Terms

It should be noted that more mechanisms than the ones described above contribute to the generation of wind waves and that other wave models include additional source terms.

For example, Booij et al. (1999) developed a model called SWAN for short-crested waves in coastal regions with shallow water. In deep water, quadruplet wave-wave interactions dominate the evolution of the spectrum (Komen et al., 1994). They transfer wave energy from the spectral peak to lower frequencies, thus moving the peak frequency to lower values. In contrast to this, in very shallow water, triad wave-wave interactions transfer energy from lower frequencies to higher frequencies (Beji & Battjes, 1993). Booij et al. (1999) included source functions for these triad wave-wave interactions in their model. Furthermore, a source function for depth-induced
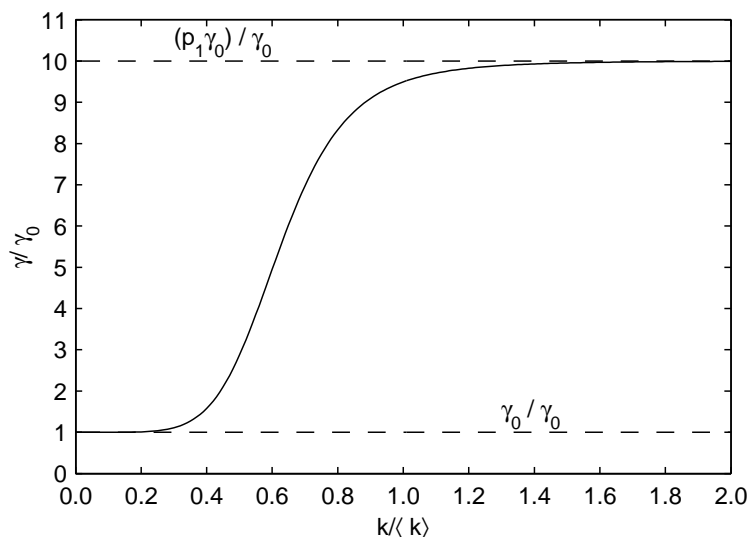
Figure 3.3: The dissipation parameter $\gamma$ of the nonlinear dissipation source function for the values given in the text (Figure adapted from Schneggenburger, 1998).

wave breaking is used in SWAN.

## 3.3  Some Remarks on Nonlinear Interactions

Nonlinear wave-wave interactions cause the redistribution of energy within the wave spectrum. If wind input and frictional dissipation were the only processes that were acting to change the energy spectrum, ocean waves would consist only of short surface waves. Apparently, long swells can also be found in the ocean which could not be generated by the wind directly. The short waves generated by Miles' mechanism begin to interact among themselves to produce longer waves (Hasselmann et al., 1973). The interactions, which are known as quadruplet or four wave interactions, transfer wave energy from short waves to waves with frequencies slightly lower than the peak frequency of the spectrum. Eventually, this leads to waves going faster than the wind, as noted by Pierson & Moskowitz (1957).

The basic principle behind the interactions is this: When the amplitude of the short waves becomes large, three waves with different wavelengths may

interact. The energy transfer is then brought about by mechanical resonance by which a fourth wavelength is created. This works only for a limited combination of waves. The resonance conditions that have to be fulfilled to make the interaction possible are

$$k_1 + k_2 - k_3 = k_4 \tag{3.17}$$

$$\omega_1 + \omega_2 - \omega_3 = \omega_4. \tag{3.18}$$

In shallow water, also triad (three wave) interactions play an important role. An example of the effect of such interactions is found when waves pass over a shallow water bank with steep lee side (see e.g. Battjes and Beji, 1993). High frequency bound waves are formed on the top of the bank and are subsequently released when the waves propagate into deeper water. These released waves then propagate independently of the main wave field. In general, the effect of the triad interactions is to make the wave frequency spectrum broader and flatter, increasing both the high frequency and the low frequency energy at the expense of the peak. Triad wave interactions are e.g. implemented in the wave model SWAN (Booij et al., 1999).

In a wave model, a full computation of the quadruplet wave-wave interactions is extremely time consuming and not convenient. A number of techniques have been proposed to improve computational speed, e.g. the discrete interaction approximation (DIA) of Hasselmann et al. (1985). The DIA has been found quite successful in describing the essential features of a developing wave spectrum in deep water (Komen et al., 1994). For the application of wave models to shallow water, a depth scaling is used for these approximations.

With regard to the K-model, Schneggenburger (1998a) accepts the significance of the four wave interactions, but he argues that the depth scaling procedure is not appropriate in very shallow water because we lack the basic understanding of how four wave interactions work in coastal seas. Therefore, we cannot give an explicit source term, and quadruplet wave interactions are neglected in the K-model.

## 3.4   Propagation and Refraction

Varying water depths and currents have an impact on the flux of wave action. As the waves propagate in a region of shallow water depths, they interact with the bottom. Thereby, properties of the waves like direction or amplitude are changed by wave propagation depending on water depths and currents.

The propagation effects can be divided into refraction, diffraction, and shoaling. Wave refraction tends to align wave crests parallel to offshore depth contours and eventually the shoreline. Wave diffraction tends to spread wave energy as a wave passes a structure or a shoal. This effect is most evident behind shore parallel breakwaters. As waves propagate past a breakwater, they bend towards the shadow zone behind the structure. Due to shoaling, the amplitude of the wave is changed (Vincent et al., 2001).

In addition to refraction due to changing water depths, waves are refracted by varying currents. Shear flows cause the waves to change their direction into the direction of the current (LeBlond & Mysak, 1978). (In section (3.6), other influences of time varying current and water level fields are described.)

In the K-model, these processes are described by the dot terms on the left-hand side of (3.1). The $\boldsymbol{x}$ gradient term represents propagation, and the $k$ and $\theta$ gradient terms refraction.

The dot terms can be derived using the dispersion function $\Omega$ for linear water waves which was given in equation (2.11) and is repeated here for convenience.

$$\Omega(\boldsymbol{k}) \;=\; \sigma(\boldsymbol{k}) \;+\; \boldsymbol{k} \cdot \boldsymbol{u}_c \tag{3.19}$$

and the kinematical relations

$$\dot{\boldsymbol{x}} \;=\; \partial_{\boldsymbol{k}}\Omega, \quad \dot{\boldsymbol{k}} \;=\; -\partial_{\boldsymbol{x}}\Omega \tag{3.20}$$

linked to $\Omega$.

The location dot terms are given by the components of the wave group velocity

$$\dot{x} \;=\; v_g \, sin\,\theta \tag{3.21}$$

$$\dot{y} \;=\; v_g \, cos\,\theta. \tag{3.22}$$

Since the group velocity is the sum of the intrinsic wave group velocity $\partial\sigma/\partial k$ and the superimposed current velocity $\boldsymbol{u}_c$, the current velocity enters the wave action balance equation through the location dot terms (3.21) and (3.22).

The $k$ and $\theta$ dot terms indicate an additional influence of the external fields on the wave dynamics. They are

$$\dot{k} \;=\; -(\sin\theta\,\partial_x\,\Omega \;+\; \cos\theta\,\partial_y\,\Omega) \tag{3.23}$$

$$\dot{\theta} \;=\; -(\cos\theta\,\partial_x\,\Omega \;+\; \sin\theta\,\partial_y\,\Omega)\,k^{-1}. \tag{3.24}$$

Water levels and currents are explicitly contained in the dispersion function. Thus, derivatives of the external fields enter the balance equation.

In the equations (3.23) and (3.24) only spatial derivatives of the dispersion function can be found. This is due to the fact that the K-model uses $(k,\theta)$ as independent $\boldsymbol{k}$-space variables. If frequency and direction $(f,\theta)$ are used instead, partial time derivatives of the disperion function appear in addition to the spatial derivatives.

In such cases, a quasi-stationary approximation can be chosen where the time dependent external fields are considered, but their partial time derivatives are neglected. However, Tolman (1990) pointed out that unsteady current and depth fields have a significant impact on surface waves. Therefore, the K-model formulation of the wave action balance equation is well suited for tidal systems as it is possible to take the non-stationarity of the external fields into account.

## 3.5   Numerical Treatment

In accordance with WAM cy. 4 (WAMDI, 1988), the K-model uses different numerical schemes for propagation and refraction terms on the one hand and for the source terms on the other hand. A time-centered implicit scheme is used for the numerical implementation of the source functions. An explicit first-order upwind scheme is used for both propagation and refraction. The upwind scheme has the disadvantage of numerical diffusion (see Komen et al., 1994). Considering swell propagation over large distances, this results in numerical dispersion. Tolman (1992) showed that in fetch-limited situations the model behaviour is hardly influenced by numerical errors in wave propagation. As fetch limitation is likely in small-scale coastal areas, Schneggenburger (1998a) concluded that the upwind scheme is suitable for the K-model.

The numerical upwind scheme is conditionally stable, i.e. the maximum allowed time step is restricted by the Courant-Friedrich-Lewy (CFL) stability criterion. The CFL criterion for combined propagation and refraction is

$$1 \geq \left| \dot{x} \frac{\Delta t}{\Delta x} \right| + \left| \dot{y} \frac{\Delta t}{\Delta y} \right| + \left| \dot{k} \frac{\Delta t}{\Delta k} \right| + \left| \dot{\theta} \frac{\Delta t}{\Delta \theta} \right| \tag{3.25}$$

where $\Delta t$ is the time step, $\Delta x$ and $\Delta y$ are the grid spacing, $\Delta k$ is the step of the modulus of the wavenumber vector, and $\Delta \theta$ is the direction step.

The model grid looks as follows: A spatial discretisation of $400\,\mathrm{m}$ is used in both horizontal directions. To discretise the $\boldsymbol{k}$-space, a logarithmic distribution of the discrete values is applied to the modulus of the wavenumber vector $k$ with $k_{i+1} = \gamma k_i$, $\gamma = 1.21$, $i = 1, ..., 25$, and $k_1 = 0.04000\,\mathrm{rad\,m^{-1}}$, $k_{25} = 3.88069\,\mathrm{rad\,m^{-1}}$. The reason for this is to obtain a better resolution of smaller values of $k$ because in the higher $k$-bins less energy is contained. For convenience, the wave lengths corresponding to the first and last $k$ values are given here, too. They are $\lambda_1 = 157.08\,\mathrm{m}$ and $\lambda_{25} = 1.62\,\mathrm{m}$. The direction of the wavenumber vector $\theta$ has been resolved by twelve different directions, starting from $15°$ with a step of $\Delta \theta = 30°$. In the K-model, both the $k$ and $\theta$ values can be chosen arbitrarily.

As water level and current fields are contained in different terms of equation (3.1), propagation and refraction can be treated separately in different subroutines with individual time steps. For propagation and refraction the time step is 2 s, for the source term integration 30 s.

## 3.6   The Influence of External Fields

As pointed out in section (3.4), surface gravity waves are influenced by varying current and water level fields. In the following, it is described in what way water levels enter the source terms and why the influence of currents on the source functions is neglected. Furthermore, some effects are specified the varying external fields have on the surface waves.

The source functions used in the K-model are all dependent on the local water depth which is explicitly contained in the source functions for bottom dissipation and nonlinear interaction. In addition, it indirectly affects all source functions via circular frequencies as well as via phase and group velocities.

In contrast to this, possible impacts of currents on the source functions are neglected in the version of the K-model used for this work. As can be seen from the fact that the intrinsic frequency $\sigma$ instead of the absolute frequency $\omega$ (equation (2.11)) is used in the equations (3.5) and (3.8), the source functions of the Phillips $S_{phil}$ and the Synder $S_{in}$ disregard the relative speed of winds and currents. Schneggenburger et al. (1997) chose this approach because the effects of currents on the source functions are not quantitatively known.
Nevertheless, an impact of the currents on the different processes described by the source functions is likely. In all likelihood the currents influence the wind input, and therefore also the turbulent eddy viscosity contained entering the nonlinear dissipation. Moreover, they contribute to the overall level of bottom stress and thus to the bottom interaction dissipation.

The waves themselves are changed by the external fields in different ways. Here, some examples are given. One phenomenon induced by varying currents is the Doppler shift. This leads to a change of integrated wave periods (for definitions of these parameters, see section 2.4).

Another example is refraction. Time varying values of water levels and currents with spatial differences result in refraction of the surface waves due to which energy is either focussed or scattered.

In addition, the significant wave height might be modified by the currents. Since the energy propagation velocity is a function of current velocity, the fetch is affected by the currents. If currents propagate in the opposing direction of the waves, the group velocity is reduced and the waves stay longer in the same area. Hence the effective fetch is increased and higher waves are generated. In contrast to this, the significant wave height is reduced by collinear currents.

Another effect of opposing currents is wave blocking. Waves propagating on strong opposing currents can be blocked by the current, creating a region downwave of the blocking point which is free of wave activity. This phenomenon can for example be encountered in tidal inlets.

# Chapter 4

# GETM

The General Estuarine Transport Model (GETM) has been used for this study to simulate the evolution of the sea surface elevation and current fields under the influence of the driving forces of wind and tides. Data yielded with GETM is used as input for the wave model. Preparation of the current and water level fields for the K-model is described in section (5.1). Here, a short description of the circulation model is presented (for a detailed disquisition on GETM, see Burchard & Bolding, 2002).

GETM was developed to simulate the dynamics of estuaries. It is especially suited for applications to shallow areas which periodically fall dry and get flooded again due to the tides. For example Stanev et al. (2002) applied GETM successfully to the whole East Frisian wadden sea.

## 4.1 Hydrodynamic equations

The fundamental equations describing motions of the ocean are governed by the incompressible Navier-Stokes equations on a rotating spherical earth with two simplifications: the hydrostatic assumption and Boussinesq approximation (see, e.g., Haidvogel & Beckmann (1999)). In the hydrostatic shallow water approximation, pressure $p$ depends only on the water depth

$$\rho g \; = \; -\partial_z p. \tag{4.1}$$

This relation holds if the horizontal dimensions of the ocean volume under consideration are much larger than the vertical dimension, hence the label 'shallow water'. According to the Boussinesq approximation, density differences are neglected unless the differences are multiplied by gravity.

In an orthogonal Cartesian coordinate system, in which $x, y$ and $z$ increase respectively eastward, westward and upward, the governing equations can be written as

$$\partial_t u + \partial_z(uw) - \partial_z\left((\nu_t + \nu)\partial_z u\right)$$

$$+\alpha\left(\partial_x(u^2) + \partial_y(uv) - \partial_x\left(2A_H^M \partial_x u\right) - \partial_y\left(A_H^M(\partial_y u + \partial_x v)\right)\right.$$

$$\left.-fv - \int_z^\eta \partial_x b\, dz'\right) = -g\partial_x \eta,$$

$$(4.2)$$

$$\partial_t v + \partial_z(vw) - \partial_z\left((\nu_t + \nu)\partial_z v\right)$$

$$+\alpha\left(\partial_x(vu) + \partial_y(v^2) - \partial_y\left(2A_H^M \partial_y v\right) - \partial_x\left(A_H^M(\partial_y u + \partial_x v)\right)\right.$$

$$\left.+fu - \int_z^\eta \partial_x b\, dz'\right) = -g\partial_y \eta.$$

$$(4.3)$$

The vertical velocity component is given by the equation of continuity

$$\partial_x u + \partial_y v + \partial_z w = 0. \qquad (4.4)$$

Equation (4.4) is the simplified form of the mass conservation equation. It has already been mentioned in chapter (2.1) and is repeated here for the sake of completeness.

In the equations (4.2) and (4.3), $f$ is the Coriolis parameter, $\nu$ the kinematic viscosity describing the molecular diffusion of momentum, and $\nu_t$ the vertical

eddy viscosity parameterizing effects of turbulent diffusion. The parameter $A_H^M$ gives a general form of he horizontal eddy viscosity coefficient. The buoyancy $b$ is known from Archimedes' principle as

$$b = -g\frac{\rho - \rho_0}{\rho_0}, \tag{4.5}$$

where $\rho$ is the density of water, and $\rho_0$ a reference density.

The terms involving the buoyancy are the internal pressure gradient which are the result of density gradients. The external pressure gradients are described by the terms with the gravitational acceleration.

When the water becomes very shallow during ebb tide the model physics are simplified by the drying and flooding parameter $\alpha$. It is given by

$$\alpha = \min\left\{1, \frac{D - D_{min}}{D_{crit} - D_{min}}\right\}. \tag{4.6}$$

In those regions of the model area where the current water depth is greater than a critical value $D_{crit}$ $\alpha$ equals unity. Then, the full model physics are allowed for. When the water depth $D = h + \eta$ approaches a lower bound $D_{min}$ $\alpha$ converges to zero. In such cases a simple balance between the external pressure gradient and friction is left. In accordance with Stanev et al. (2002) the minimum allowable water depth $D_{min}$ is 5 cm and the critical value $D_{crit}$ is 20 cm.

## 4.2   Boundary conditions

The kinematic boundary condition for the surface was given in equation (2.4) and is repeated here for convenience in terms of the velocity vector v=(u,v,w)

$$w = \partial_t\eta + u\partial_x\eta + v\partial_y\eta \qquad \text{for } z = \eta. \tag{4.7}$$

At the bottom, the kinematic boundary condition reads

$$w = -u\partial_x h - v\partial_y h \qquad \text{for } z = -h. \tag{4.8}$$

At the bottom the horizontal velocity components follow the 'no slip' condition

$$u = 0, \quad v = 0, \quad w = 0. \tag{4.9}$$

The vanishing of the horizontal velocity components at the bottom implies the existence of frictional boundary layers because the velocity is brought to zero from the free stream values across a thin boundary layer where friction is important.

At the surface, the dynamic boundary conditions are given by

$$(\nu_t + \nu)\partial_z u = \alpha\tau_s^x, \tag{4.10}$$

$$(\nu_t + \nu)\partial_z v = \alpha\tau_s^y, \tag{4.11}$$

where $\tau_s^x$ and $\tau_s^y$ indicate the surface stresses being for example dependent on wind features. The surface stresses are multiplied by the factor $\alpha$ in order to incorporate the flooding and drying due to the tides.

## 4.3   Vertically Integrated Mode

Since only two-dimensional velocity and sea surface elevation fields are needed as input for the wave model, GETM has been used in the vertically integrated mode.

Under consideration of the kinematic boundary conditions (4.7) and (4.8) the vertical integration of the equation of continuity yields the sea surface elevation equation

$$\partial_t \eta = -\partial_x U - \partial_y V \tag{4.12}$$

with

$$U = \int_{-h}^{\eta} u \, dz, \qquad V = \int_{-h}^{\eta} v \, dz \,. \tag{4.13}$$

After vertically integrating the horizontal equations of motion read

$$\partial_t U + \tau_b^x + \alpha \left( \int_{-h}^{\eta} \left( \partial_x u^2 + \partial_y (uv) \right) \, dz \right.$$

$$- \tau_s^x - \int_{-h}^{\eta} \left( \partial_x \left( 2A_H^M \partial_x u \right) - \partial_y \left( A_H^M (\partial_y u + \partial_x v) \right) \right) dz \qquad (4.14)$$

$$\left. - fV - \int_{-h}^{\eta} \int_z^{\eta} \partial_x b \, dz' \, dz \right) = -gD\partial_x \eta$$

and

$$\partial_t V + \tau_b^y + \alpha \left( \int_{-h}^{\eta} \left( \partial_x (uv) + \partial_y v^2 \right) \right) dz$$

$$- \tau_s^y - \int_{-H}^{\eta} \left( \partial_y \left( 2A_H^M \partial_y v \right) - \partial_x \left( A_H^M (\partial_y u + \partial_x v) \right) \right) dz \qquad (4.15)$$

$$\left. + fU - \int_{-h}^{\eta} \int_z^{\eta} \partial_y b \, dz' \, dz \right) = -gD\partial_y \eta.$$

The water depth $D$ on the right-hand side of the equations equals $\eta - (-h)$.

## 4.4 Numerical Treatment

The barotropic mode of GETM comprises the surface elevation equation (4.12) and the transport equations (4.14) and (4.15). When discretising these equations, the presence of the gravity waves and the sea surface leads to severe time step limitations. As the vertically integrated equations are treated explicitly, the time step has to obey the following stability criterium

$$\Delta t < \left[ \frac{1}{2} \left( \frac{1}{\Delta x} + \frac{1}{\Delta y} \right) \sqrt{2gD} \right]^{-1}. \qquad (4.16)$$

In this study a time step of $9\,\mathrm{s}$ has been used.

For the spatial discretisation a staggered Arakawa C-grid is used (Arakawa & Lamb, 1977) with a grod box width of $200\,\mathrm{m}$. In the following, this grid is described for the variables $U$, $V$ (mass transports) and $\eta$ (sea surface elevation), the variables needed as an input for the wave model.

The C-grid is composed of three subgrids. The first subgrid shows a mesh for the variable $\eta$, the second shows a mesh for the variable $U$ (West-East transport), and the third shows a mesh for the variable $V$ (North-South Transport). The overlay comprises the staggered grid in such a way that $\eta$ is located at the center of the mesh boxes, and the mass transports $U$ and $V$ are displaced half a grid box to the west of the center and half a grid box to the south of the center, respectivly (see figure (4.1)).
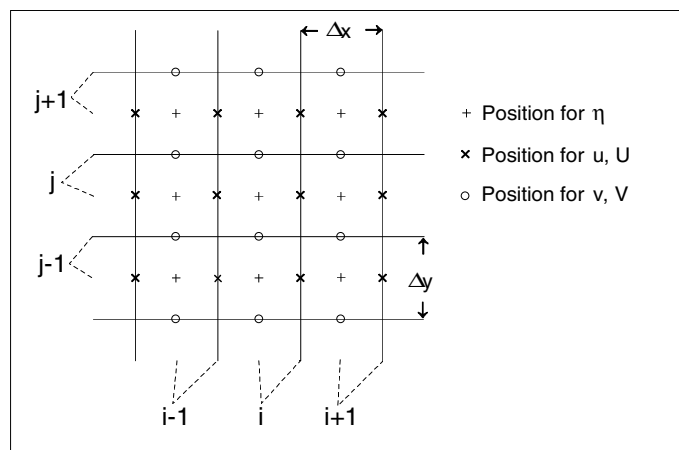


Figure 4.1: The horizontal Arakawa C-grid of GETM (the figure has been adapted from Burchard & Bolding (2002))

# Chapter 5

# Model Setup

In the following chapter the model setup is laid out. Firstly, the one-sided coupling of the K-model with the current model is described. Secondly, the model domain is presented. The chapter concludes with a description of the forcing for the two models composed of the wind data used for both models, the tidal forcing for GETM, and the boundary spectra for the wave model.

## 5.1   Coupling of the Two Models

In order to couple the wave model with the current model, the current velocity and sea surface elevation fields were linearly interpolated from the Arakawa C-grid of GETM to the non-staggered, simple grid of the K-model. For the sea surface elevation four T-Points of the C-grid were averaged yielding a value in the middle of the former four. To take into account possible land and dry points, the involved dry points were counted. If their number was greater than two the value in the middle was set to a dry point. Otherwise, the average of the wet points was calculated.

For the interpolation of the current velocities only those values of the C-grid were considered that are located directly above and below the K-model grid points in the case of the velocity component $u$, and directly left and right to the K-model grid point in the case of the velocity component $v$.

The interpolation procedure is depicted in figure (5.1). The obtained in-

terpolated values were converted into timeseries data files of the new grids
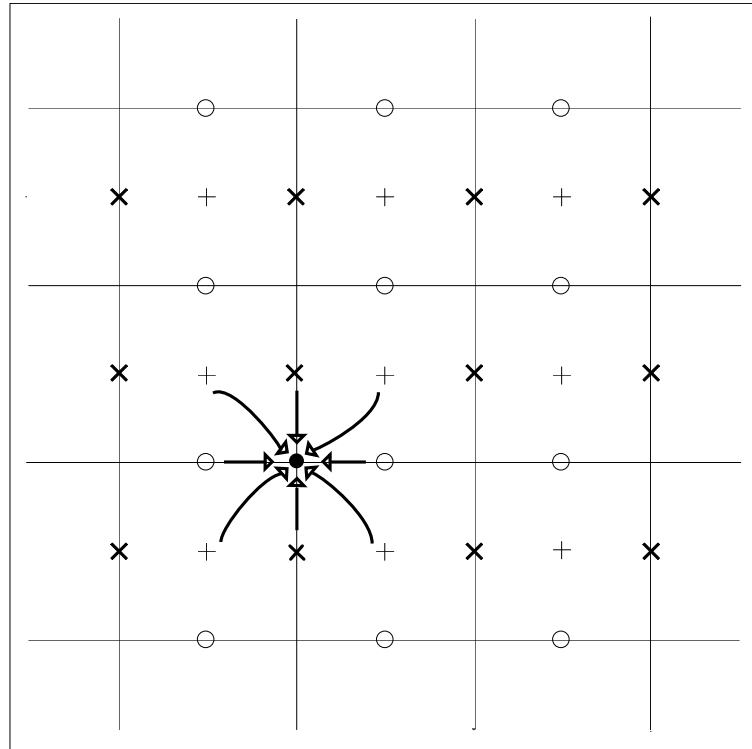which then were used as model forcing for the wave model.



Figure 5.1: Illustration of the interpolation from the
Arkawa C-grid of the current model to the non-staggered
grid of the wave model. The arrows indicate which val-
ues were taken into account.

The coupled model has been applied to the wind scenarios described in
section(5.4). Simulations have been carried out with and without taking
time varying currents into account. The model output comprises current
velocities, surface elevation fields, integrated wave parameter fields, and
frequency-direction spectra and time series of integrated wave parameter
for the positons depicted in (5.3).

## 5.2   Model Area

The wadden sea is a shallow sea extending along the North Sea coasts from
Den Helder, the Netherlands, and to Esbjerg, Denmark, with an overall
length of about 500 km. In the mean, the wadden sea is about 10 km wide and

covers a total area of about $8\,000\,\mathrm{km}^2$. The German part amounts to about 50% of this area. It comprises the coastal area of the German Bight and ranges from the most western East Frisian barrier island Borkum to the island Sylt in front of the western coast of Schleswig-Holstein (cf. figure (5.2)).
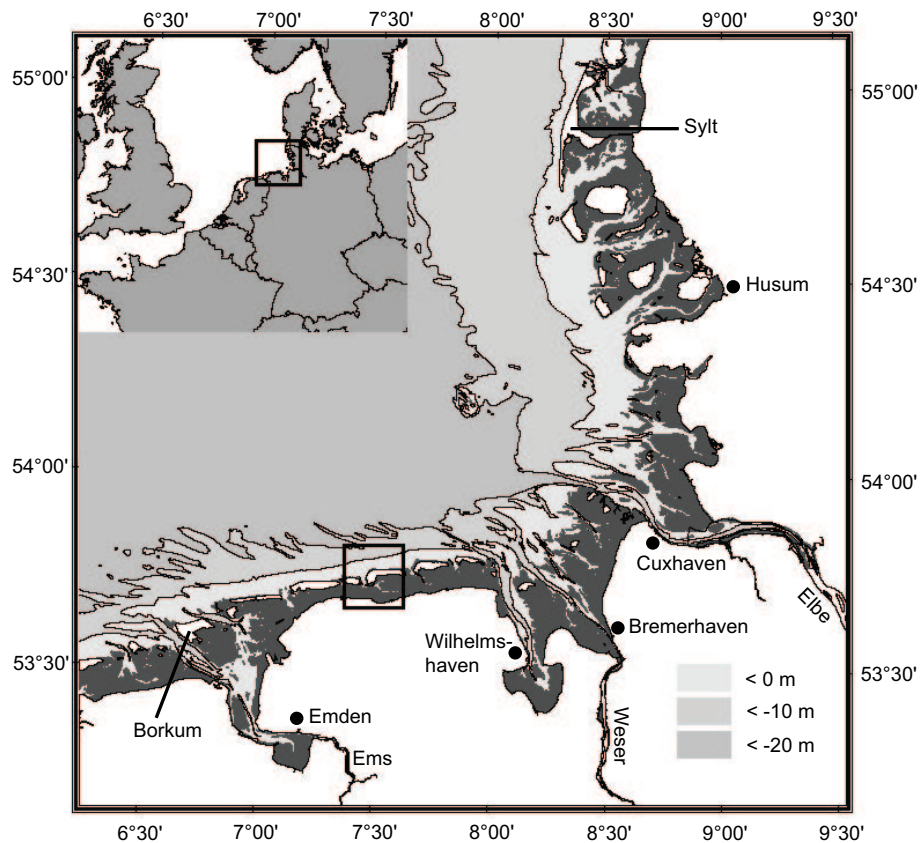


Figure 5.2: Map of the North Sea and the German Bight. The inset depicts the North Sea with the German Bight margined by the square. In the big map of the German Bight the square delimits the model area. The dark shading marks approximately the part of the German Bight that periodically falls dry. (The figure has been adapted from Stanev et al. (2002).)

The behaviour of water motion and geomorphology in the Wadden Sea is strongly controlled by the tides. In the German part, the tidal range varies between 2.2 m in Borkum and 3.6 m in Wilhelmshaven. During low tides large parts of the wadden sea emerge. These so-called tidal flats cover a large portion of the tidal area and are one of its most characteristic features.

During high tides the flats are inundated again.

The wadden sea has a complex bathymetry, consisting of tidal inlets with the associated tidal deltas, tidal flats, and a network of channels and shoals. Typical tidal velocity amplitudes in the inlets are of the order of $1\,\mathrm{ms}^{-1}$ (Wolff, 1983). The morphology in the wadden sea varies depending on the wave and tidal conditions which constitute the hydrographic regime. Wave driven littoral transport moves and redistributes sediment parallel to the coast that has been carried perpendicular towards the coast by the tides. The littoral drift is predominantly eastward directed. A classification of the relationship between the hydrographic regime and the coastal morphology was given by Hayes (1979). It is assumed in this classification that with increasing tidal energy the importance of wave energy decreases. According to Hayes (1979), the coast can be divided into microtidal, mesotidal, and macrotidal areas. The German wadden sea is partly mesotidal and partly macrotidal. Where the tidal range is greater than 2.90 m, the conditions are macrotidal. The littoral transport is minimal so that sandy barriers are few. Therefore, the size of the barrier islands increases with a decreasing mean tidal range towards the outer German Bight (Dijkema et al., 1980). Where the tidal range exceeds 1.35 m, the conditions are mesotidal. Tidal flats separate the coast from barrier islands which are intersected by tidal inlets. Through the inlets a large amount of sediment is carried and deposited on both the oceanward (ebb tidal delta) and shoreward (flood tidal delta) side.

The coupled model has been applied to the part of the German wadden sea around the two barrier islands Baltrum and Langeoog. Approximating the inter-tidal basin connected to the North Sea via the tidal inlet called 'Accumer Ee', the area of the wadden sea between the two islands and the East Frisian coast, together with about 6.5 km of the open North Sea in front of the islands has been considered as model area. Its topography is shown in figure (5.3). The model domain is 15.2 km long and 15.6 km wide. Morphological features consist of a tidal inlet, tidal channels, and tidal flats. The tidal range is about 2.5 m (Niemeyer, 1994). According to the classification set forth above, this area is mesotidal.

The required topography was provided by Gerhard Gayer from the Institute

for Coastal Research at the GKSS Forschungszentrum. He used measuring data acquired by the Federal Waterways Engineering and Research Institute (BAW) in the year 1995. The distance between the measuring points varied between 250 m on the seaward side of the area, and 20 m near the deeper tidal channels. Between theese points G. Gayer interpolated linearly and obtained a topography with resultion of 100 m in both horizontal directions. For the simulations with the current model which uses an Arakawa C-grid the topography data was interpolated to a $200 \times 200$ m grid with $76 \times 78$ gridpoints. Calculations with the wave model have been conducted with a $400 \times 400$ m grid with $76 \times 78$ gridpoints. The data was also obtained by interpolating. The grid of the K-model is not staggered.
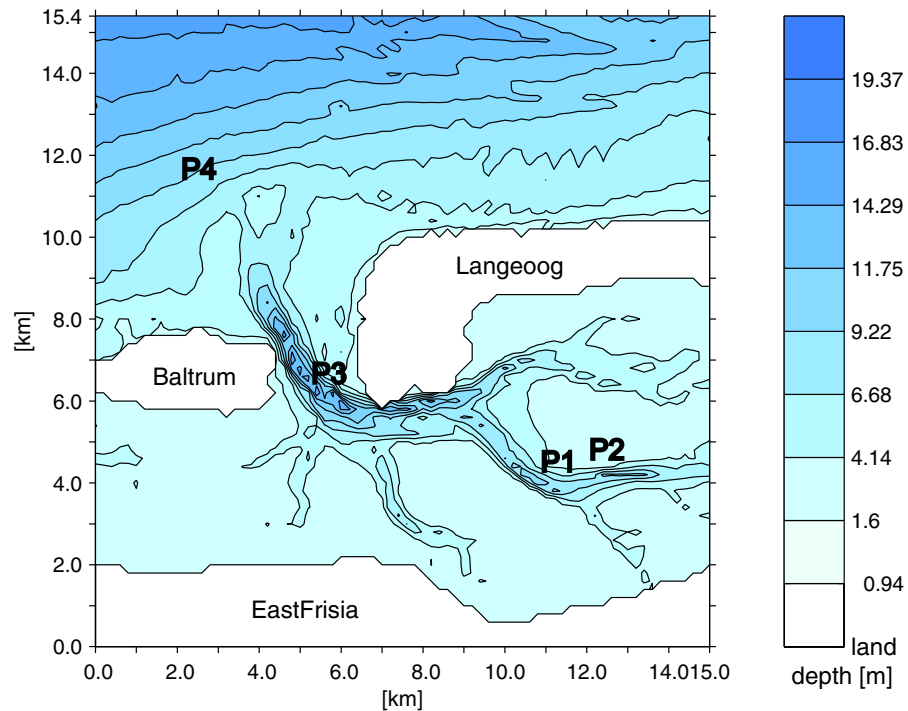


Figure 5.3: The topography of the model area.

## 5.3 The Tides

At the open boundaries on the northern, western, and eastern edge of the model area sea level data has been prescribed to account for the

influence of the tides. The data was calculated by the German Federal Maritime and Hydrographic Agency (Bundesamt für Seeschiffahrt und Hydrographie, BSH) with a three-dimensional prognostic model (Dick & Sötje, 1990). Simulations are carried out of the North Sea and Baltic Sea with a horizontal resolution of 10 km, and of the German Bight with a higher resolution of 1.8 km.

The sea level data was calculated from 14 tidal constituents. In the wadden sea, the semi-diurnal lunar tide M2 with a period of 12.42 h and the semi-diurnal solar tide S2 with a period of 12.00 h are predominant. Interaction between these solar and lunar tides results in spring tides and neap tides depending on wether the Sun and Moon are in syzygy or in quadrature.

The available time series of sea level data starts on the May 19$^{th}$, 2000. The temporal resolution is 15 min. In figure (5.4), the first seven days of the sea level time series are shown. With these values simulations have been carried out. The red dot approximately marks when the spring tide set in.
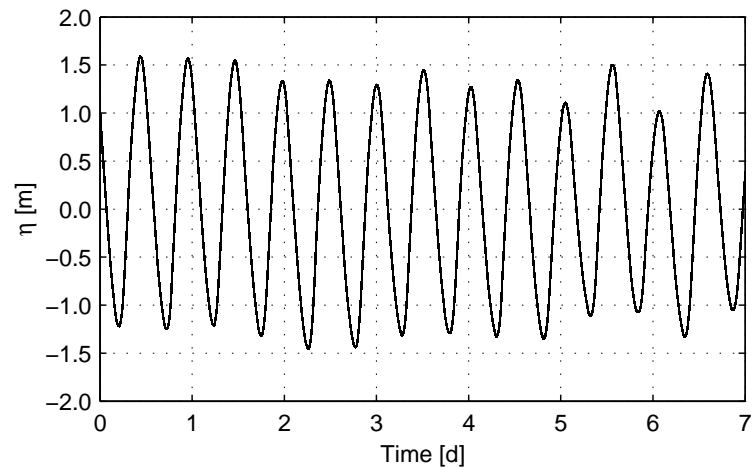


Figure 5.4: Time series of sea level data.

When prescribing the boundary values for the sea surface elevation, we have to take the phase shift in the tidal rise and fall due to the amphidromy in the southern North Sea into consideration. The tidal wave propagates through the North Sea as a Kelvin wave, in this case in a counter-clockwise circular motion. This leads to patterns of high and low tides rotating around amphidromic points at which the tidal rise and fall is zero. The German wadden sea is under the influence of the amphidromic system whose point of zero tidal rise is located approximately at 55° 27'N - 5° 18'E (Tomczak & Godfrey, 1994). The associated tidal wave propagates along the Belgian and Dutch coast in a northerly direction towards Germany and Denmark.

Stanev et al. (2002) conducted simulations for the whole East Frisian wadden sea. Their model domain has a total length of 65 km. The corresponding phase shift is approximately 50 min. The length of the model area under investigation in this thesis is 15 km. For simplicity a linear relationship has been assumed between the phase shift of the tidal wave along an area of the wadden sea coast and the length of this area. Subsequently, the phase shift for the Baltrum-Langeoog area is taken to be 11.5 min.
In order to resolve this phase shift in the boundary values, two successive sea level values in the data set have been interpolated in time yielding a value that has a phase difference of 11.5 min to the later original value. These two values were allocated to the two northern corners of the model area. Between these two values, an interpolation in space was carried out to obtain the boundary values needed for the grid point along the northern boundary. The boundary values on the western and eastern boundary have been held constant, the western boundary equal to the northwestern sea level value, and the eastern boundary equal to the northeastern sea level value.

## 5.4   Wind Input

As wind input a constant wind velocity for the whole model domain was chosen. Case studies are carried out for four different wind scenarios. These were obtained from measured data that was acquired by the GKSS with a hydrographic pile. The position of the pile is R 2596081.575 and H 5954395.026 in Gauss-Krüger coordinates and is marked in figure (5.3).

The period of measurement started at 15.03.2001, 18:50 and ended at 19.11.2001, 14:50.

The wind data given by wind speed and direction was evaluated in the following way: The direction given by a 360° clockwise scale with 0° in northern direction was divided into twelve direction 'bins' each 30° wide. The wind speed data contained in each direction bin was subdivided into four speed bins with an interval of $5.0\,\mathrm{ms}^{-1}$. The wind data in such a combined direction-speed bin were averaged. From the averaged direction-speed bins four different wind velocities were chosen. The criteria of the choice were that the speeds have a maximum magnitude and that the four directions differ sufficiently.

Figure (5.5) shows the wind velocities in the averaged bins. Please note that 180° were added to the wind direction to give an impression where the winds were blowing to. The length of the arrows corresponds to the magnitude of the wind speeds ranging from $2.98\,\mathrm{ms}^{-1}$ to $17.23\,\mathrm{ms}^{-1}$.

It is pointed out here that the wind velocities used in this thesis are not representative of the East-Frisian wadden sea. The monthly averages of the wind speeds do not exceed $8.0\,\mathrm{ms}^{-1}$ (C. Lefebvre, DWD, pers. comm.). In the analysed time series, the chosen winds are not among the most frequent ones. In table (5.1) the frequencies with which data sets occur in one direction-speed bin are listed to give an impression of this.

In GETM, the constant winds were included by giving the corresponding constant wind stresses which were computed using the bulk formular

$$\tau \;=\; C_D u_{10}^2 \rho \tag{5.1}$$

together with the formula for the drag coefficient suggested by Smith & Banke (1975)

$$C_D \;=\; (0.63 + 0.066 u_{10}) \times 10^{-3}. \tag{5.2}$$

The K-model applies the wind velocities by calculating the source terms described in (3.2.1.1) and (3.2.1.2).
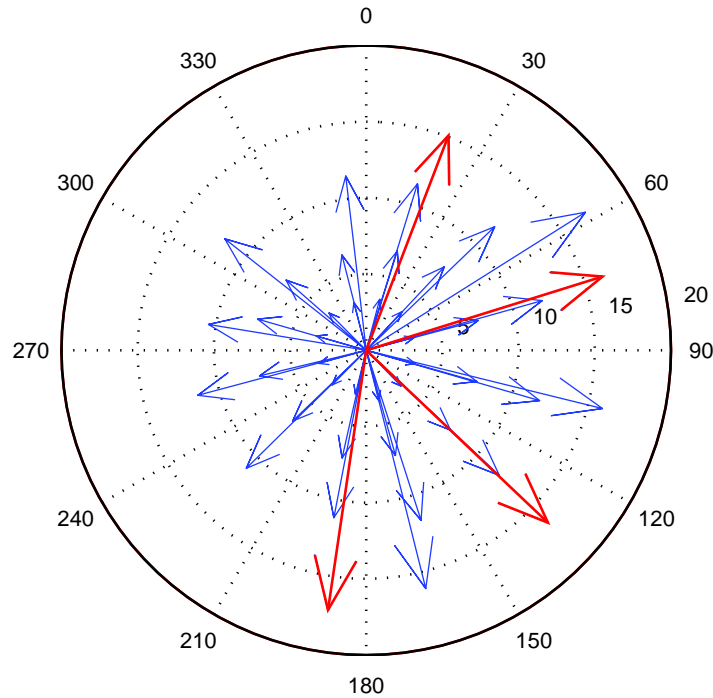
Figure 5.5: Average wind velocities in the direction-speed bins. The velocities chosen for the case studies are presented in red color.

Table(5.2) gives the wind velocities and corresponding stresses used for case studies.

## 5.5   Boundary Spectra

For the simulations with the K-model boundary spectra were prescribed on the open boundaries. The spectra were calculated in such a way that they represent the chosen wind scenarios described in section (5.4). To this end, representative fetch lengths and water depths were assumed for the different wind velocities (table (5.3)). These take into account the areas the winds are coming from. The discrete wave numbers given in section (3.5) were converted to the respective frequencies using the deep-water dispersion relation. Using a simple directional distribution, two-dimensional TMA spectra were calculated for these frequency, depth, and fetch values. The obtained energy densities were converted to action densities depending on the wave number.

Table 5.1: Frequencies of data-sets in the direction-speed bins.

| | 0-5 ms$^{-1}$ | 5-10 ms$^{-1}$ | 10-15 ms$^{-1}$ | 15-20 ms$^{-1}$ |
|---|---|---|---|---|
| **0°-30°** | 1291 | 960 | 299 | 25 |
| **30°-60°** | 1068 | 804 | 33 | 0 |
| **60°-90°** | 880 | 1352 | 537 | 0 |
| **90°-120°** | 961 | 1636 | 129 | 0 |
| **120°-150°** | 1130 | 629 | 132 | 0 |
| **150°-180°** | 1251 | 676 | 62 | 0 |
| **180°-210°** | 1431 | 1895 | 410 | 1 |
| **210°-240°** | 977 | 2531 | 870 | 13 |
| **240°-270°** | 682 | 1813 | 782 | 65 |
| **270°-300°** | 815 | 2203 | 633 | 84 |
| **300°-330°** | 672 | 1312 | 929 | 397 |
| **330°-360°** | 994 | 1102 | 353 | 36 |

(for an explanation of TMA spectra, cf. A.4.3).

Table 5.2: The wind velocities and corresponding stresses used for case studies. The wind velocities are given in polar and Cartesian coordinates, the wind stresses in Cartesian coordinates.

|  | $|\boldsymbol{u}_{10}|$ [ms$^{-1}$] | **Dir.** [°] | $u_{10}$ [ms$^{-1}$] | $v_{10}$ [ms$^{-1}$] | $\tau_x$ [Nm$^{-2}$] | $\tau_y$ [Nm$^{-2}$] |
|---|---|---|---|---|---|---|
| S1 | 15.09 | 21.0 | 5.4078 | 14.0877 | 0.1659 | 0.4321 |
| S2 | 16.44 | 133.5 | 11.9252 | -11.3165 | 0.4203 | -0.3988 |
| S3 | 16.24 | 72.7 | 15.5053 | 4.8294 | 0.5357 | 0.1668 |
| S4 | 17.23 | 188.4 | -2.5170 | -17.0452 | -0.0958 | -0.6488 |

Table 5.3: Representative fetches and water depths chosen for the boundary spectra.

|  | Fetch X [km] | Depth [m] |
|---|---|---|
| S1 | 20 | 5 |
| S2 | 1 200 | 40 |
| S3 | 500 | 20 |
| S4 | 500 | 35 |

It should be noted, that the used forcing data is not consistent. The starting time of the boundary values for the sea surface elevation is 19$^{\text{th}}$ May 2000. The analysed time series of the hydrographic pile starts on the 15$^{\text{th}}$ March 2001. Nevertheless, the different data sets reflect real processes. A tidal range of about 2.5-3.0 m is likely in the East Frisian wadden sea, and so are wind speeds of about 15 ms$^{-1}$. The combination of these inconsistent data sets is therefore justified.

# Chapter 6

# Results

## 6.1 Directional Spectra

One objective of this thesis is to investigate the influence of the current fields on the waves. For this reason, a selection of frequency-direction spectra are shown here.

Spectra are given here for the positions P2, P3 and P4. The tidal inlet represented by the position P3 is very well suited to point out the current effects because the current speeds are the highest there. Therefore, the influence on the waves, if there is any, should be obvious. Spectra of the positions P2 and P4 are presented to show deviations in the spectra brought about by different depth. Figure (6.1 (a) and (b)) are good examples how the Doppler shift due to the currents influences the waves and consequently the spectra. The current induced Doppler shift is a term in the absolute frequency $\omega$ given in equation (2.11). If the current and wave directions are nearly diametrical, the scalar product $\boldsymbol{k} \cdot \boldsymbol{u}_c$ converges to a negative minimum. Then, the absolute frequency is reduced. This can be seen in figure (6.1). Current and wave directions are opposed. Therefore, the spectrum contains more energy in the lower frequencies. The contrary is depicted in figure (6.2) where current and waves directions are about the same giving rise to wave frequncies being shifted to higher values. Moreover, the spectrum is broadened in the former case figure (6.1), and narrow in the latter figure (6.1).

The situation shown in figure (6.1 a and b) describes the refraction by cur-

rents. The current and wave directions are perpendicular to each other, and the waves are diverted to the directions of the currents.

Comparing figure (a and b) it is obvious that the energy content in the spectrum at position P2 is less than in the spectrum at P4. As the position P2 is located on the tidal flats, more wave energy is dissipated by bottob friction than at the sea and position P4.
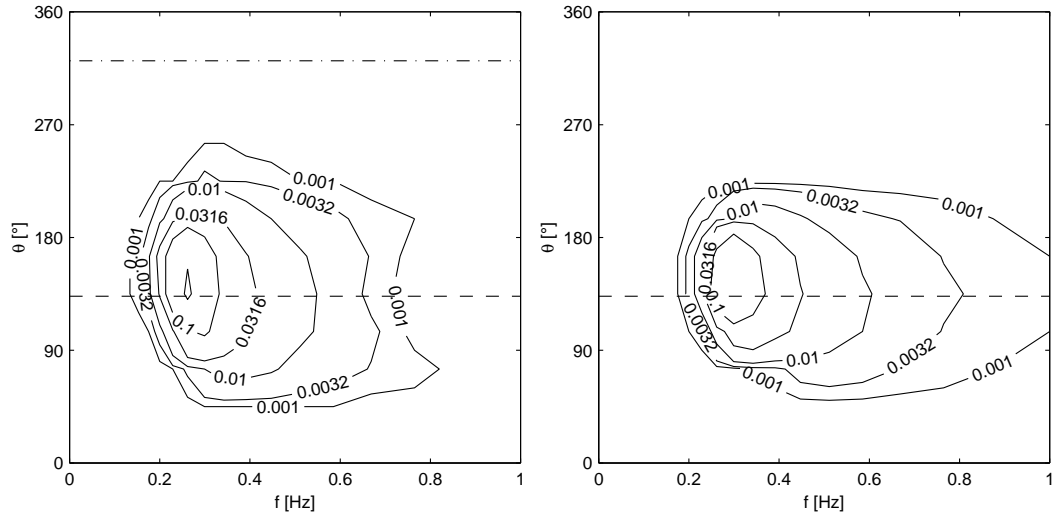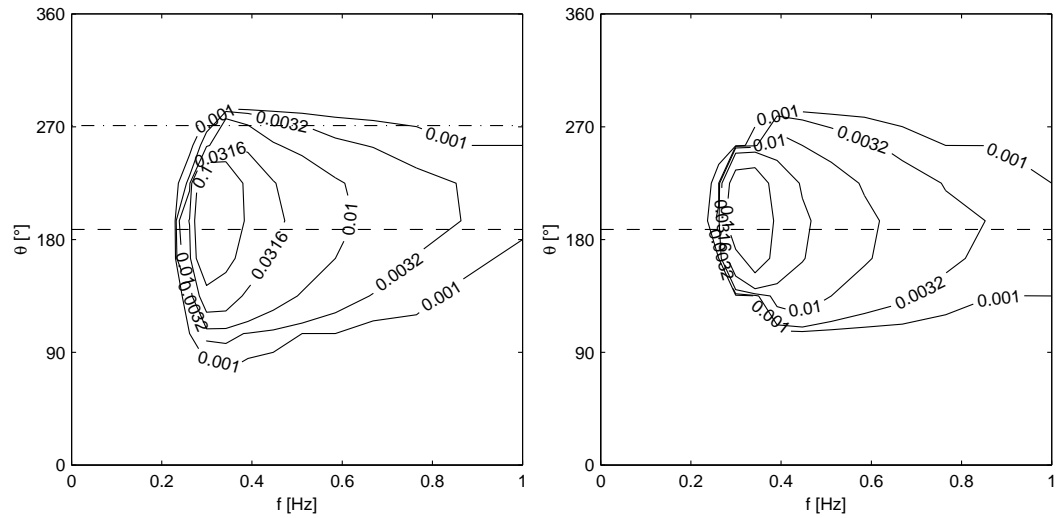
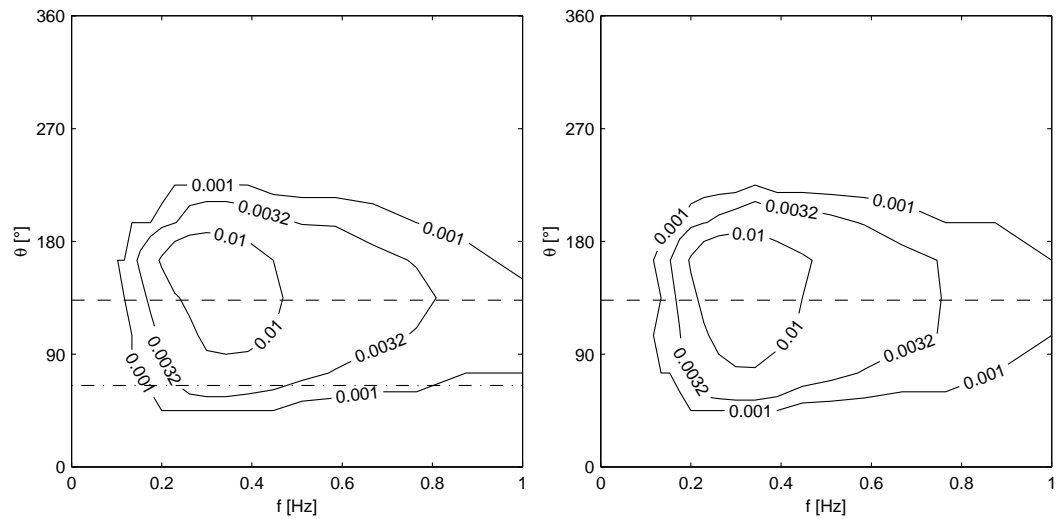(a) P3 inlet, wind scenario S2, three hours after high tide
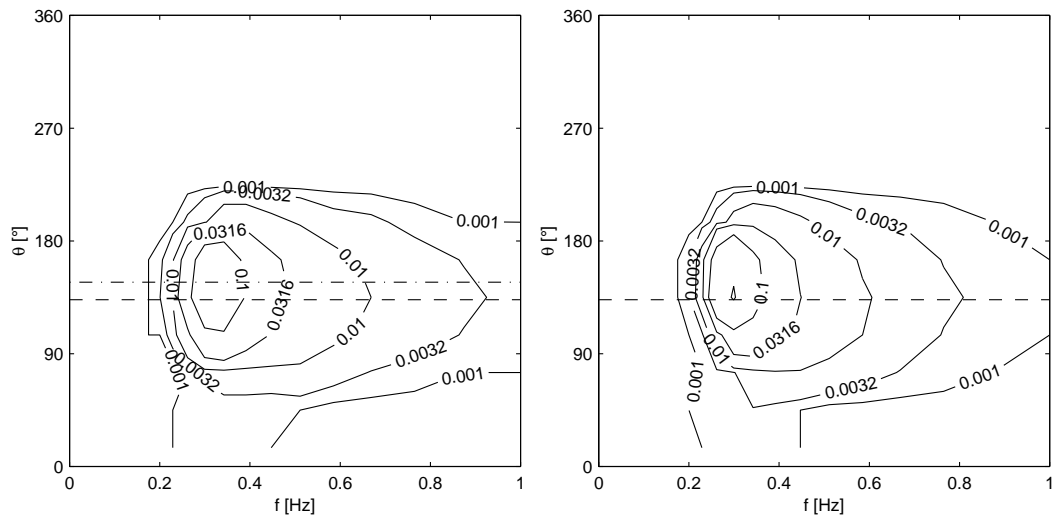


(b) P3 inlet, wind scenario S2, one hour before high tide

Figure 6.1: Selected frequency-direction spectra for the locations and times given in the captions of each plot. The left panels show spectra for the simulations with varying currents, and the right panels without currents. Contour line intervals are logarithmic. Spectral Energy densities are given in $m^2Hz^{-1}$. Dashed lines represent the wind directions, dot-dashed lines the current directions.

(a) P4 frontisland, wind scenario S4, three hours after high tide



(b) P2 flat, wind scenario S2, two hours after high tide

Figure 6.2: Annotation as in figure (6.1).

## 6.2   Time Series

In this section, the effects on wave parameters brought about by currents are illustrated by time series of these parameters and current parameters. To this end, four different time series are discussed, each of them put out at a different location and for a different wind scenario. The locations are shown in figure (5.3) The first panel shows the influence on the significant wave height $H_s$, the second panel on the $T_{m1}$ wave period. The dashed lines indicate the changes in time without currents, the solid lines with currents. The third and fourth panel demonstrate how current directions and current velocities change with the tides. The dotted lines in the third panels give the directions of the currents.

Figure (6.3) presents the time series for the wind scenrio S2 (north-western direction) at the location P4. The two upper panels show the impact of currents on the significant wave height and the integrated parameter $T_{m1}$. As both parameters stay nearly constant when current is not taken into account for the simulation, the influence of tidal currents can clearly be seen. The current velocities shown in the fouth panel have no severe difference for ebb and flood periods. The value of the current velocities is around $0.25\,\text{ms}^{-1}$. The varitions of $T_{m1}$ are greater when the current directions and the wave directions are anti-parallel. The parameter $T_{m1}$ reaches its minimum when wave directions and current directions are equal.

Figure (6.4) shows the time series at the location P2 and for the wind scenario S1 with southern wind. As can be seen from the time series the significant wave height $H_s$ and the integrated $T_{m1}$ equals zero during ebb tide. This is not unlikely as the water depth at this position is shallow. The current influence on these parameters is negligible, because the dashed and solid lines do not differ. Again, it can be pointed out that the opposite current and wave directions have an effect on the integrated parameter $T_{m1}$. A small bulge is notable at time points 20 and 08. For the current velocities in the fouth panel can be said that the run of the curve is similar to the modulus function due to the fact that current that the current directions change to the opposite. During ebb tide no or little water is found at

the position P2, hence no data has been computed, since the wave model requires a minimum water depth of 0.5 m.

At the loction P3 for the wind scenario S4 (northern wind) a distinction of the tides is evident (see figure (6.6). The current influence on the significant wave height is completely negligible because the curves for both versions can be regarded similar. The current directions change suddenly with the changing of the tides. This is most obvious for the position P3. The tidal influence on the current velocity is also visible in the last panel where the values of the velocities vary from $0.27\,\mathrm{ms}^{-1}$ to $0.0\,\mathrm{ms}^{-1}$. Again, it can be pointed out that opposite wave directions and current directions amplify the range ot the parameter $T_{m1}$.

In figure (6.5) the last time series at location P1 for the wind senario S3 (south-western wind) is presented. As expected for this position the significant wave height $H_s$ has no severe amplitude. It can be regarded as constant. As the wave directions and the current directions are parallel most of the time the integrated parameter curve is as well nearly constant. The different simulations, one includes current input, the other does not, can hardly be distinguished from each other. The current velocities are small like in the first figure (6.3). Their maximum value is $0.25\,\mathrm{ms}^{-1}$.

At the end of this time series representation, it is worth to mention that current influences occur periodically with the tides. In all four cases the effects are roughly identical.
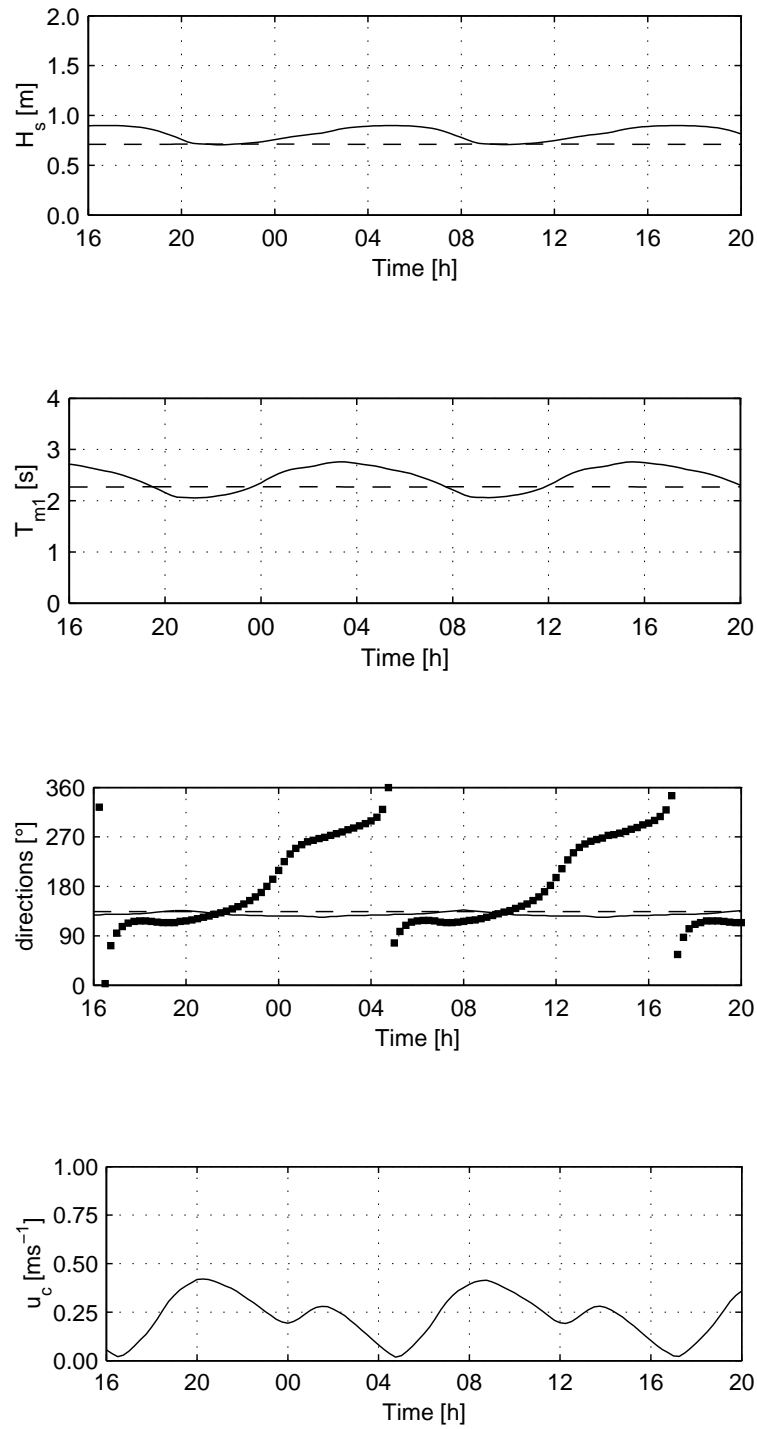
Figure 6.3: Time series of integrated wave parameters and the current velocities for the the wind scenario S2 at the location P4. The solid lines represent the simulations with currents included, and the dashed lines without currents. The dotted line in the bottom panel gives the current direction.
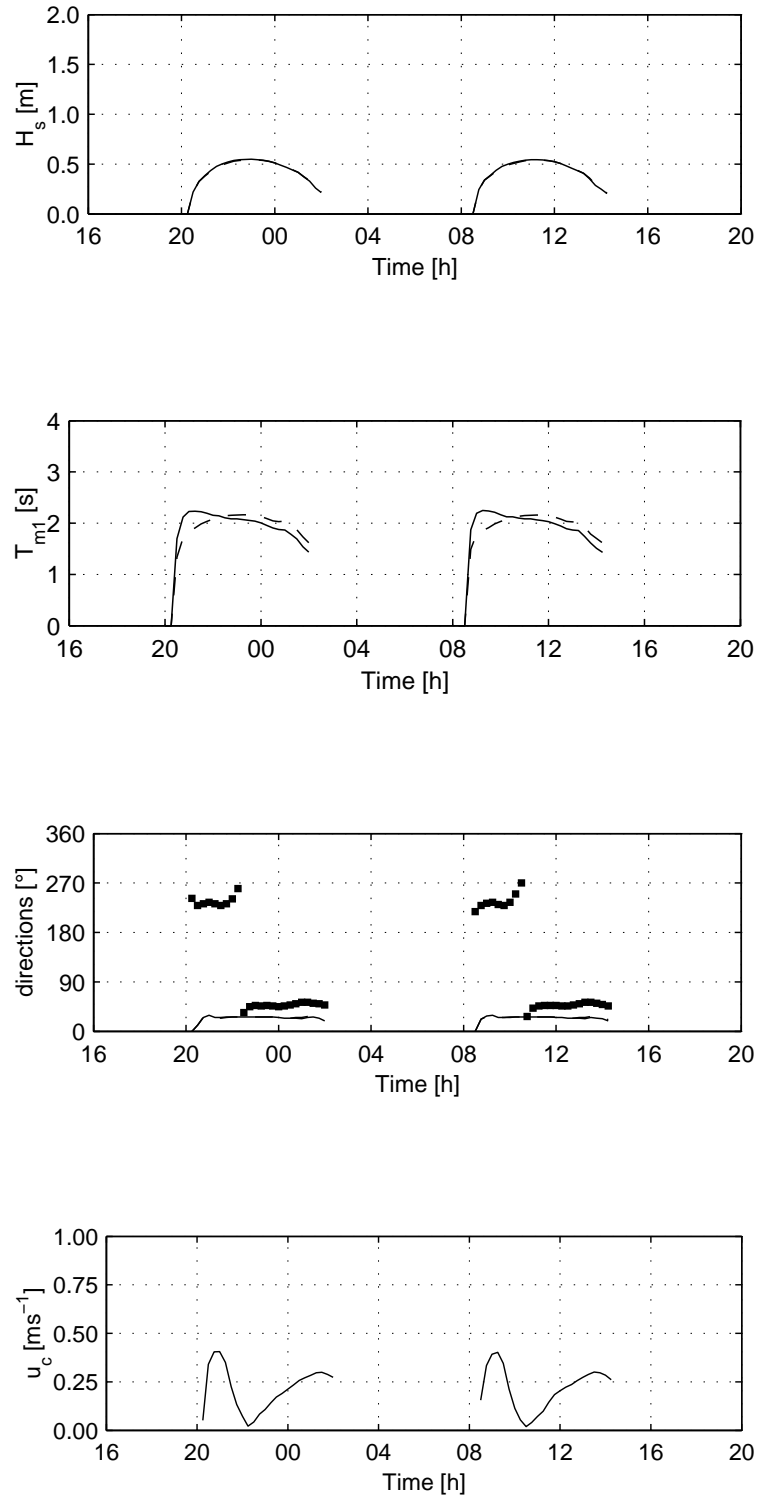
Figure 6.4: Time series of integrated wave parameters and the current velocities for the the wind scenario S1 at the location P2. Line style as in figure (6.3).
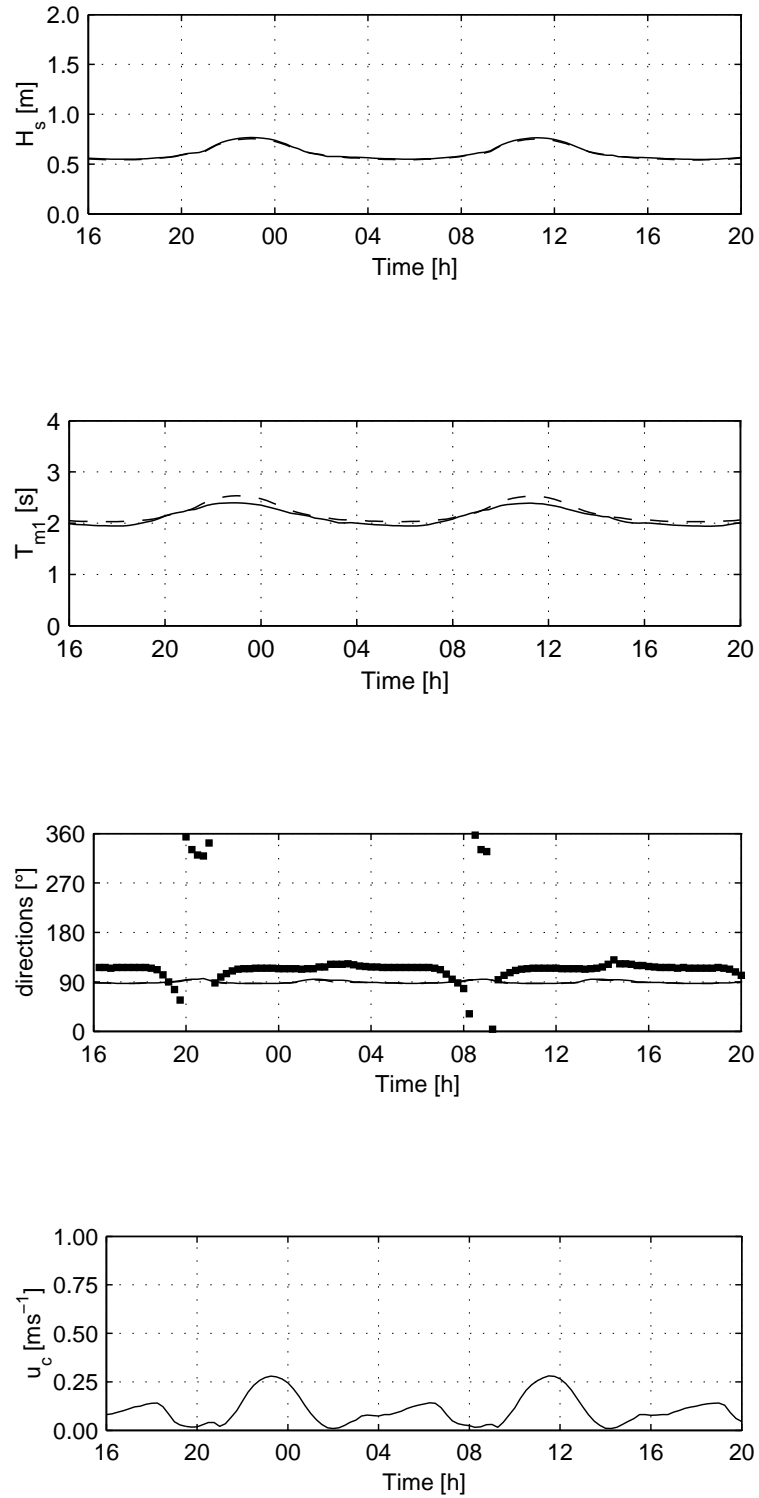
Figure 6.5: Time series of integrated wave parameters and the current velocities for the the wind scenario S3 at the location P1. Line style as in figure (6.3).
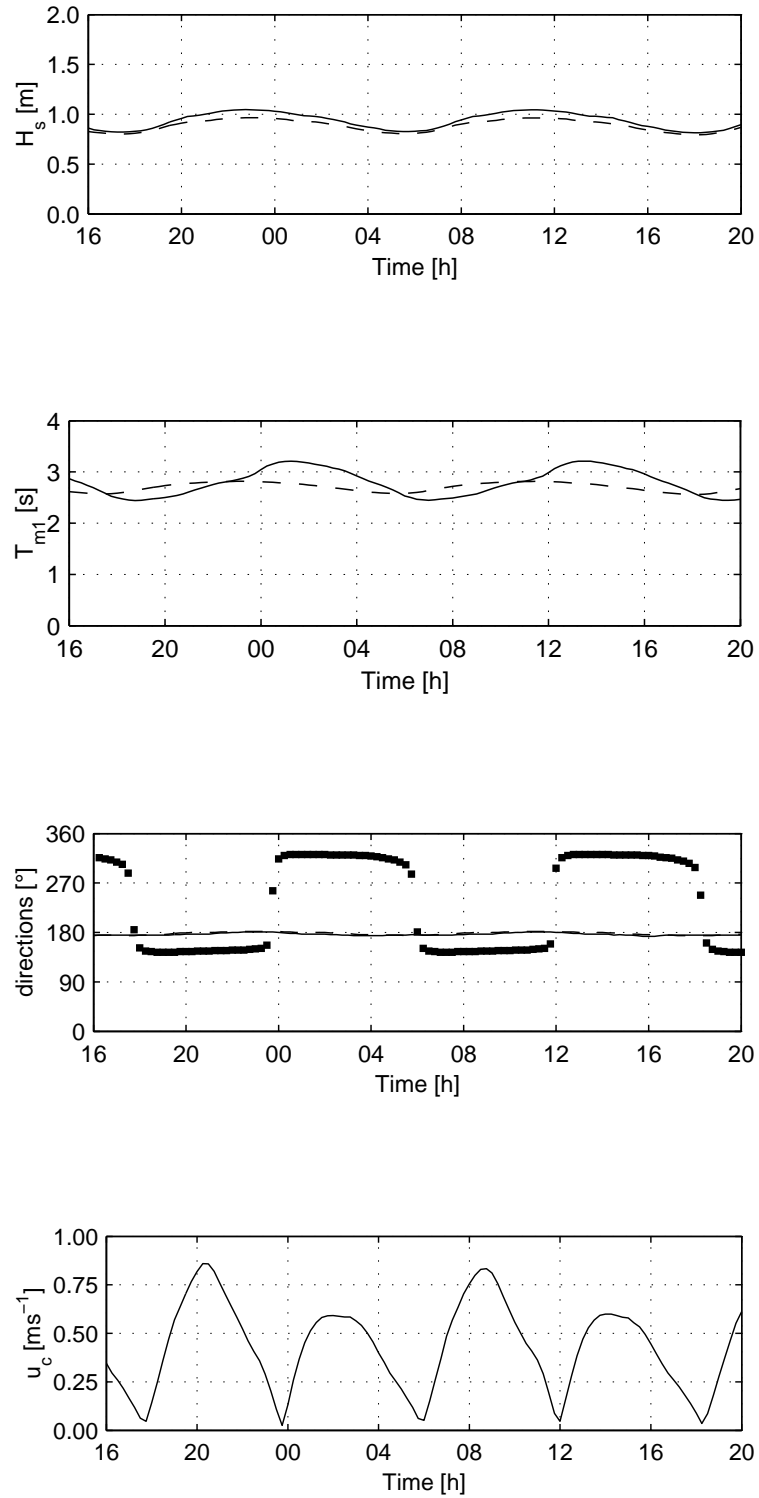
Figure 6.6: Time series of integrated wave parameters and the current velocities for the the wind scenario S4 at the location P3. Line style as in figure (6.3).

## 6.3 Integrated Wave Parameter and Current Fields

In order to get an impression of how the differences between the four scenarios, and, at the time, of how current fields affect the wave fields , here the obtained model results are depicted as field plots. These show the model area with the East Frisian coast and the two barrier islands Baltrum and Langeoog. On the following two pages, each column of plots represents one wind scenario. In each column the panel at the top shows the modulus of the current velocities and the velocities as stream lines. The center panel presents wave height fields computed with current input. To allow an estimation of the current influence the ave heights obtained without the currents included in the ave model are shown in the bottom panel. All firlds describe the condition of the water shortly before high tide. The units of the scales to the right of the plots are $ms^{-1}$ in the case of the velocity fields, and $0.1\,m$ in the case of the water heights. The arrows indicate the wave directions.

Depending on where the wind is coming from it enhances or weakens the current pattern induced by the tides. For example, in the current velocity plot of scenario S1 the current velocities in the tidal basin are rather small, and the currents are rather slowly propagating through the inlet (cf. top left panel of figure (6.7)). In comparison to this, under the influence of the wind of scenario S2 the velocities are higher in the inlet and in the basin (cf. top right panel of figure (6.7)). Since the plots show the status of the fields shortly before high tide, the influence of the winds is probably stronger than during full developed ebb or flood currents. Therefore, this effect might be overstated by the plots. The strong tidal currents are not likely to be deflected or hampered by the winds.

Concerning the influence of the currents on the waves only slight differences are detectable for the cases S1 and S3. For the other two cases the two lower panels vary. When currents are taken into consideration the wave heights are generally higher. It seems that for the case S4 waves are advected by the currents in front of the inlet on the seaward side, and that the waves are caught there.

Besides the interaction of the waves with the currents, depth refraction can

be seen in most wave height-directions plots. South of Langeoog this phenomenon is visible in the middle and bottom panel of figure (6.8). As the waves turn towards the island in both plots, this cannot be due to the currents. Depth refraction is a likely explanation.

In addition to the impacts of changing depths and currents, the shadowing effects of the islands are evident in plot of the wave height. Depending on the direction of the wind, waves are smaller on the respective leeward side of the islands.
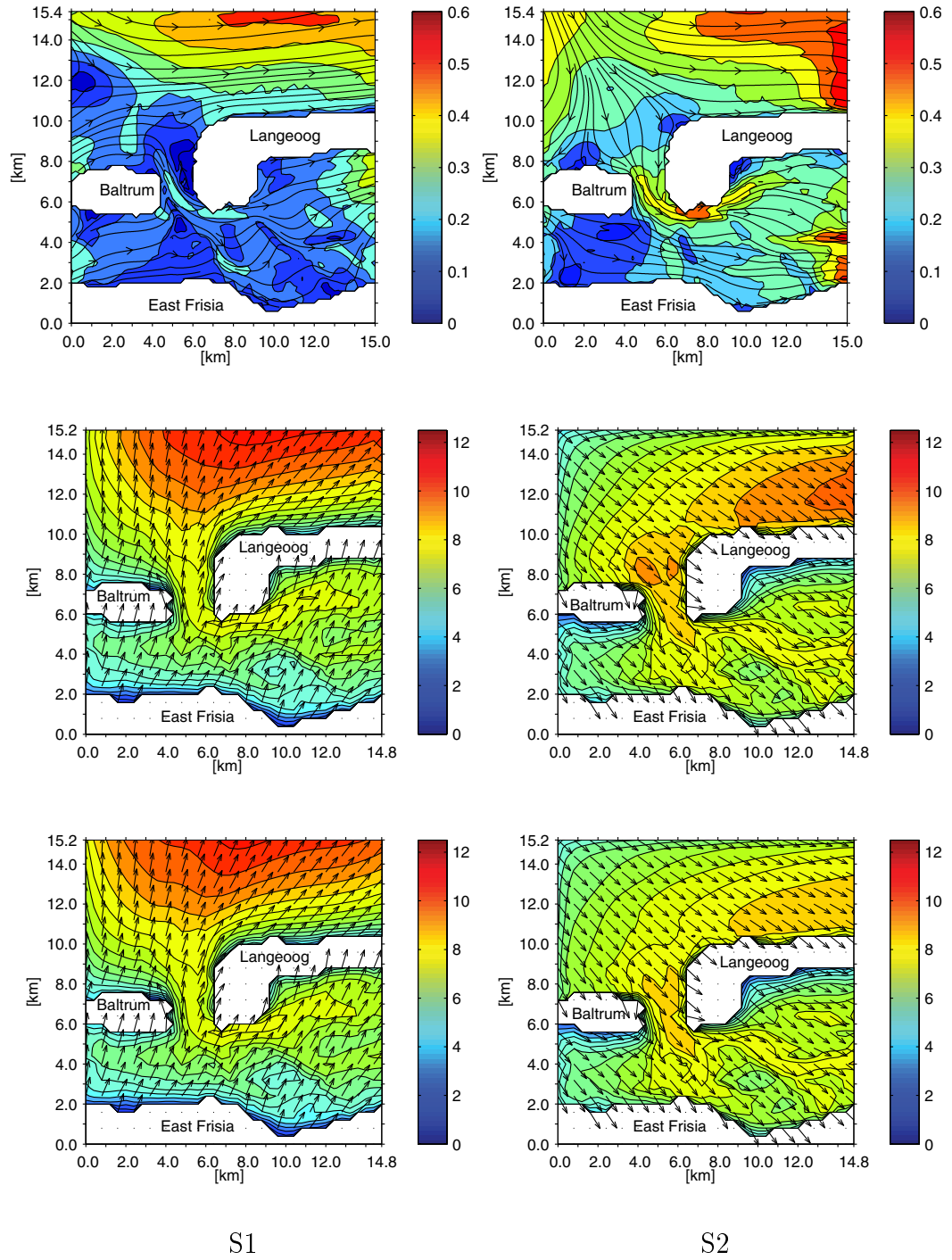
S1                                    S2

Figure 6.7: Fields of the current velocity and the significant wave height for the stated scenarios
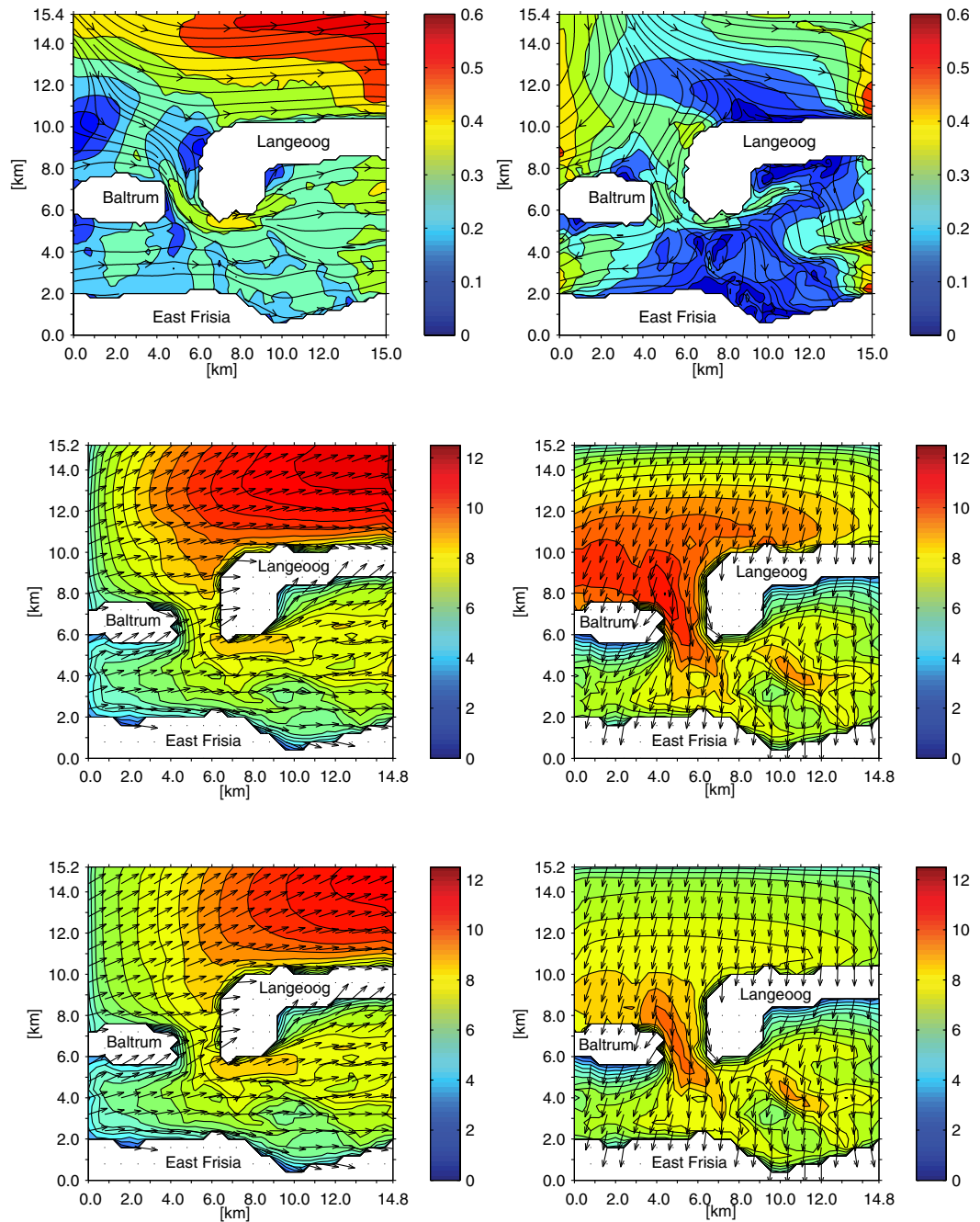
Figure 6.8: Fields of the current velocity and the significant wave height for the stated scenarios

# Chapter 7

# Conclusions

This study on the effects of tidal currents and different wind scenarios on wind waves in the East Frisian wadden sea give rise to the following conclusions:

For the East Frisian wadden sea, modulations of mean wave parameter such as the significant wave height and the mean wave periods can be significant depending on the position and the tidal and meteorological conditions.

The simulations of the different wind situations produced expected results. The interesting part is the interplay of the wind induced waves with the tidal currents.

Even though inconsistent forcing data has been used, realistic physical processes could be successfully approximated.

# Chapter 8

# References

Arakawa,A., and V.R. Lamp, Computational design of the basic dynamical processes of the UCLA General Circulation Mode, *Meth. Comput. Phys.*, pp. 173-263, 1977

Bauer, H., 1991: Wahrscheinlichkeitstheorie, De Gruyter, Berlin.

Beji, S., and J.A. Battjes, 1993: Experimental investigation of wave propagation over a bar, *Coastal Eng.*, **19**, 151-162.

Booij, N., R. C. Ris, and L. H. Holthuijsen, 1999: A third-generation wave model for coastal regions. Part I: Model description and validation. *Journal of Geophysical Research*, **104**, 7649-7666.

Bouws,E., and G.J. Komen, 1983: On the balance between growth and dissipation in an extreme depth-limited wind sea in southern north sea, *J. Phys. Oceanogr.*, **13**, 726-750

Bouws,E., H. Günther, W. Rosenthal, and C.L. Vincent, 1985: Similarity of the wind wave spectrum in finite depth water. 1. Spectral form. *J. Geophys. Res.*, **90(C1)**, 975-986.

Bretherton, F.P., and C.J.R. Garret, 1968: Wave trains in inhomogeneous moving media. *Proc. Roy. Soc. London*, **A302**, 529-554.

Burchard, H., and K. Bolding, 2002: GETM - a general estuarine transport model. Scientic documentation, *Tech. Rep. EUR 20253 EN*, European Commission.

Cavaleri, L., and P.M. Rizzoli, 1981: Wind wave prediction in shallow water - theory and application, *J. Geophys. Res.*, **86**, 10961-10973.

Christoffersen, J.B., and I.G. Jonsson, 1985: Bed friction in a combined current and wave motion. *Ocean Engineering*, **12**, 387-423.

Demirbilek, Z., and C.L. Vincent, 2002: Water Wave Mechanics, in Coastal Engi-

neering Manual, US Army Corps of Engineers.

Dijkema, K.S., H.-E. Reineck, and W.J. Wolff, 1980: Geomorphology of the Wadden Sea area, in *Ecology of the Wadden Sea*,W.J. Wolff, Ed., Balkema, Rotterdam 1/1-1/135, 1983

Donelan, M.A., and Y. Yuan, 1994: Wave dissipation by surface processes, in *Dynamics and Modelling of Ocean Waves*, G.J. Komen et al., Eds., Cambridge University Press, 143-155.

Haidvogel, D.B., and A. Beckmann, 1999: Numerical Ocean Circulation Modeling (Series on Environmental Science and Management). *Imperial College Press*, London, England.

Hayes, M., 1979: Barrier island morphology as a function of tidal and wave regime, in *Barrier Islands from the Gulf of St. Lawrence to the Gulf of Mexico*, S.P. Leatherman Ed., Academic Press, NY, pp. 1-29

Hasselmann, K., and J.I. Collins, 1968: Spectral dissipation of finite-depth gravity waves due to turbulent bottom friction, *J. Mar. Res.*, **26**, 1-12.

Hasselmann, K., T.P. Barnett, E. Bouws, H. Carlson, D.E. Cartwright, K. Enke, J.A. Ewing, H. Gienapp, D.E. Hasselmann, P. Krusemann, A. Meerburg, P. Müller, D.J. Olbers, K. Richter, W. Sell, and H. Walden, 1973: Measurements of wind-wave growth and swell decay during the Joint North Sea Wave Project (JONSWAP), *Dt. Hydrogr. Z. Suppl.*, **A 8 (12)**, 95p.

Hasselmann, K., 1974: On the spectral dissipation of ocean waves due to white capping, *Boundary-Layer Meteorol.*, **6**, 107-127

Hasselmann, D.E.,M. Dunckel, and J. A. Ewing, 1980: Directional wave spectra observed during JONSWAP 1973, *J. Phys. Oceanogr.*, **10**, 1264-1280.

Hasselmann, S., and K. Hasselmann, 1985a: Computations and Parametrizations of the nonlinear energy transfer in a gravity wave spectrum, part 1: A new method for efficient computations of the exact nonlinear transfer integral, *J. Phys. Oceanogr.*, **15**, 1369-1377

Janssen, P.A.E.M., 1989: Wave induced stress and the drag of air flow over sea waves, *J. Phys. Oceanogr.*, **19**, 745-754

Komen, G.J., L. Cavaleri, M. Donelan, K. Hasselmann, S. Hasselmann, and P.A.E.M. Janssen, 1994: Dynamics and Modelling of Ocean Waves, Cambridge University Press.

LeBlond, P.H., and L.A. Mysak, 1978: *Waves in the Ocean*, Elsevier oceanography series, Elsevier, Amsterdam.

Lefebvre, C., DWD, *pers. Comm.*, Average wind velocities in the German wadden sea.

Miles, J.W., 1957: On the generation of surface waves by shear flows, *J. Geophys. Res.*, **99**, 18501-18511.

Mitsuyasu, H., 1975: Observations of the directional spectrum of ocean waves using a cloverleaf buoy, *J. Phys. Oceanogr.*, **5**, 750-759.

Phillips, O.M., 1957: On the generation of waves by turbulent wind, *J. Fluid Mech.*, **2**, 417-445.

Phillips, O.M., 1977: *The Dynamics Of The Upper Ocean*, Cambridge University Press.

Pierson, Jr., W.J., and L. Moskowitz, 1964: A proposed spectral form for fully developed wind seas based on the similarity theory of S. A. Kitaigorodskii, *J. Geophys. Res.*, **69**, 5181-5190.

Rosenthal, W., 1989: Derivation of Phillips $\alpha$-parameter from turbulent diffusion as a damping mechanism, in *Radar Scattering from Modulated Wind Waves*, G.J. Komen and W.A. Oost, Ed., Kluwer Academic Publishers, 81-88.

Schneggenburger, C., 1998a: Spectral wave modelling with nonlinear dissipation, PhD thesis, University of Hamburg, *GKSS external report 98/E/42*.

Schneggenburger, C., H. Günther, W. Rosenthal 1998b: Shallow water wave modelling with nonlinear dissipation: application to small scale tidal systems. in *Proc. 5th Int. Workshop Wave Hindcasting and Forecasting*, 242-255, Melbourne, Florida

Schneggenburger, C., 1997: Shallow water wave modelling with nonlinear dissipation, *Dt. Hydrogr. Z.*, **49**, 431-444.

Schneggenburger, C., H. Günther, W. Rosenthal 2000: Spectral wave modelling with non-linear dissipation: validation and applications in a coastal tidal environment, *Coastal Engineering*, **41**, 201-235.

Shemdin, O., K. Hasselmann, S.V. Hsiao and K. Herterich, 1978: Non-linear and linear bottom interaction effects in shallow water, p347-372, in *Turbulent fluxes through the sea surface, wave dynamics and prediction*, A. Favre and K. Hasselmann, Eds., Plenum, New York 677p.

Smith, S. and E. G. Banke, 1975: Variation of the sea surface drag coefficient with wind speed. *Q. J. Royal Meteor. Soc.*, **101**, 665-673.

Snyder, R.L., F.W. Dobson, J.A. Elliot and R.B. Long, 1981: Array measurements of atmospheric pressure fluctuations above surface gravity waves, *J. Fluid*

*Mech.*, **102**, 1-59.

Stanev, E., J.-O. Wolff, H. Burchard, K. Bolding, and G. Flöser, On the circulation in the East Frisian wadden sea: Numerical modelling and data analysis, *Ocean Dynamics*, 2002, submitted.

Tolman, H.L., 1990 The influence of unsteady depth and currents of tides on wind-wave propagation in shelf seas *J. Phys. Oceanogr.*, **20**, 1166-1174.

Tolman, H.L., 1992: Effects of numerics on the physics in a third-generation wind-wave model, *J. Phys. Oceanogr.*, **22**, 1095-1111.

Tomczak, M., and J.S. Godfrey, 1994: Regional Oceanography: an Introduction. Pergamon, New York, 422 pages

Vincent C.L., Z. Demirbilek, and J.R. Weggel, 2001: Estimation of Nearshore Waves, in Coastal Engineering Manual, US Army Corps of Engineers.

WAMDI group: S. Hasselmann, K. Hasselmann, E. Bauer, P.A.E.M. Janssen, G.J. Komen, L. Bertotti, P. Lionello, A. Guillaume, V.C. Cardone, J. A. Greenwood, M. Reistad, L. Zambresky, and J.A. Ewing, 1988: The WAM model - a third generation ocean wave prediction model, *J. Phys. Oceanogr.*, **18**, 1775-1810.

Weber, S.L., 1994: Bottom friction and percolation, p156-166, in *Dynamics and Modelling of Ocean Waves*, G.J. Komen et al., Eds., Cambridge University Press, 532p

Whitham, G.B., 1974: Linear and non-linear waves. Wiley, New York, 636p.

Willebrand, J., 1975: Energy transport in a nonlinear and inhomogeneous random gravity wave field, *J. Fluid Mech.*, **70**, 113-126.

W.J. Wolff, 1983: Ecology of the Wadden Sea

# Appendix A

# Wave Spectra

## A.1 Wavenumber-directional Spectrum

**Offshore Hydrodynamics: Spectrum Axis Transformation**

Converting the wavenumber vector to polar coordinates the wave spectrum can be given by

$$F(k,\theta) \;=\; k\,F(\boldsymbol{k}). \tag{A.1}$$

It now depends on $k$, the modulus of the wavenumber vector, and $\theta$ denoting the direction of the wavenumber vector. $\theta$ is measured clockwise from north.

This representation is called the wavenumber-direction spectrum. It has numerical advantages for spectral wave modelling. Using the discrete wavenumber-direction spectrum the directional resolution does not depend on the wave number $k$. Hence, the same directional resolution is applied when resolving wave energy in different wavelength bins (Schneggenburger, 1998a).

## A.2 Frequency-directional Spectrum

A common spectral representation of the three-dimensional sea surface is to consider the frequency-directional spectrum $F(f,\theta)$, which represents how

the variance is distributed in frequency $f$ and direction $\theta$.

$$F(f, \theta) \;=\; \frac{2\pi k}{v_D} \, F(\boldsymbol{k}) \tag{A.2}$$

Although $F(f, \theta)$ is actually a measurement of variance (cf. paragraph 2.1.2), $F(f, \theta)$ is called the 2-D or directional energy spectrum because it can be multiplied by $\rho g$ to obtain wave energy (Komen et al., 1994). The advantage of this representation is that it tells us in what direction the wave energy is moving.

It is often convenient to express the directional spectrum $F(f, \theta)$ describing the angular distribution of wave energy at respective frequencies by

$$F(f, \theta) \;=\; F(f)D(f, \theta) \tag{A.3}$$

where the function $D(f, \theta)$ is a dimensionless quantity which is known as the directional distribution or the directional spreading function (Demirbilek et al., 2002). The one-dimensional frequency spectrum $F(f)$ is explained below.

The functional form of the directional distribution $D(f, \theta)$ has no universal shape. Proposals were made e.g. by Mitsuyasu et al. (1975) and Hasselmann (1980). Mitsuyasu et al. (1975) proposed a form that varies with wave frequency and is related to the stage of wave development.

## A.3   Frequency Spectrum

If directional information is lacking, it is suitable to work with the one-dimensional frequency spectrum. The frequency spectrum may be obtained by integrating the associated directional spectra over $\theta$

$$F(f) \;=\; \int_0^{2\pi} F(f, \theta) \, d\theta. \tag{A.4}$$

$F$ is equal to the Fourier transform of the temporal correlation function

$$F(f) \;=\; \int_0^{\infty} e^{-2\pi i f \tau} \langle \eta(\boldsymbol{x}, t + \tau) \, \eta(\boldsymbol{x}, t) \rangle \, d\tau. \tag{A.5}$$

Therefore, $F(f)$ can be determined from a time series measurement in a single point (Komen et al., 1994).

$F(f)$ is often called the one-dimensional or frequency energy spectrum because the energy of the wave field may be estimated by multiplying $F(f)$ by $\rho g$. Hence, a wave spectrum tells us what frequencies have significant energy content (Demirbilek et al., 2002).

## A.4   Parametric Spectra

In general, the spectrum of the sea surface does not follow any specific mathematical form. However, under certain wind conditions the spectrum does have a specific shape. A series of empirical expressions have been found which can be fit to the spectrum of the sea surface elevation. These are called parametric spectra.

### A.4.1   Pierson-Moskowitz Spectrum

A well-known parametric spectrum is the single-parameter spectrum of Pierson-Moskowitz PM (Pierson and Moskowitz 1964).

The equilibrium form of the PM spectrum for fully-developed seas may be expressed in terms of wave frequency $f$ and wind speed $U_w$ as

$$F_{PM}(f) = \frac{0.0081 g^2}{(2\pi)^4 f^5} \exp\left[-0.24\left(\frac{2\pi U_w f}{g}\right)^{-4}\right] \tag{A.6}$$

where $U_w$ is the wind speed at 19.5 m above mean sea level. The PM spectrum describes a fully-developed sea with one parameter, the wind speed, and assumes that both the fetch and duration are infinite. This idealization is justified when wind blows over a large area at a constant speed without substantial change in its direction for tens of hours.

An important value in wave modelling is the Pierson-Moskowitz frequency which gives the peak frequency of the PM spectrum.

### A.4.2   JONSWAP Spectrum

An extension of the PM spectrum is the JONSWAP spectrum. The JONSWAP spectrum for fetch-limited seas was obtained from the Joint North

Sea Wave Project (JONSWAP) (Hasselmann et al. 1973) and may be expressed as

$$F_J(f) \;=\; \frac{ag^2}{(2\pi)^4\,f^5}\,\exp\left[-\frac{5}{4}\left(\frac{f}{f_m}\right)^{-4}\right]\gamma^{\exp\frac{-(f-f_m)^2}{2\sigma^2 f_m^2}} \tag{A.7}$$

with

$$f_m \;=\; 3.5\left(\frac{g^2 F}{U_{10}^3}\right)^{-0.33}, \quad \alpha_J \;=\; 0.076\left(\frac{gX}{U_{10}^2}\right)^{-0.22}, \quad 1 \;\le\; \gamma_J \;\le\; 7. \tag{A.8}$$

In this equation, the Phillips constant $\alpha_J$ is a scaling parameter, $f_m$ the frequency at the spectral peak, $U_{10}$ the wind speed at the elevation 10 m above the sea surface and $X$ the fetch length. The peak enhancement factor $\gamma_J$ gives the ratio of spectral peak energy to the Pierson-Moskowitz peak energy. The parameter $\sigma_J$ defines the peak width. Commonly, $\sigma_J$ is split up into two values: $\sigma_a$ for the forward face and $\sigma_b$ for the rear face of the spectrum

$$\sigma_J \;=\; \begin{cases} \sigma_a & \text{for} \quad f \le f_m \\ \sigma_b & \text{for} \quad f > f_m\,. \end{cases} \tag{A.9}$$

Figure (A.1) qualitatively illustrates the relationship between PM and JONSWAP spectra.

## A.4.3 TMA Spectrum

Bouws et al. (1985) proposed a parametric for water wave spectra in finite depth water, the TMA spectrum. They analysed spectra from different data sets (T = Texel, M = Marsen = Marine Remote Sensing Experiment and A = Arsloe = Atlantic Ocean Remote Sensing Land-Ocean Experiment). The TMA Spectrum was developed to incorporate finite depth effects into the JONSWAP spectrum.

$$F_{TMA}(f) \;=\; \psi(f,h)\,F_J(f) \tag{A.10}$$

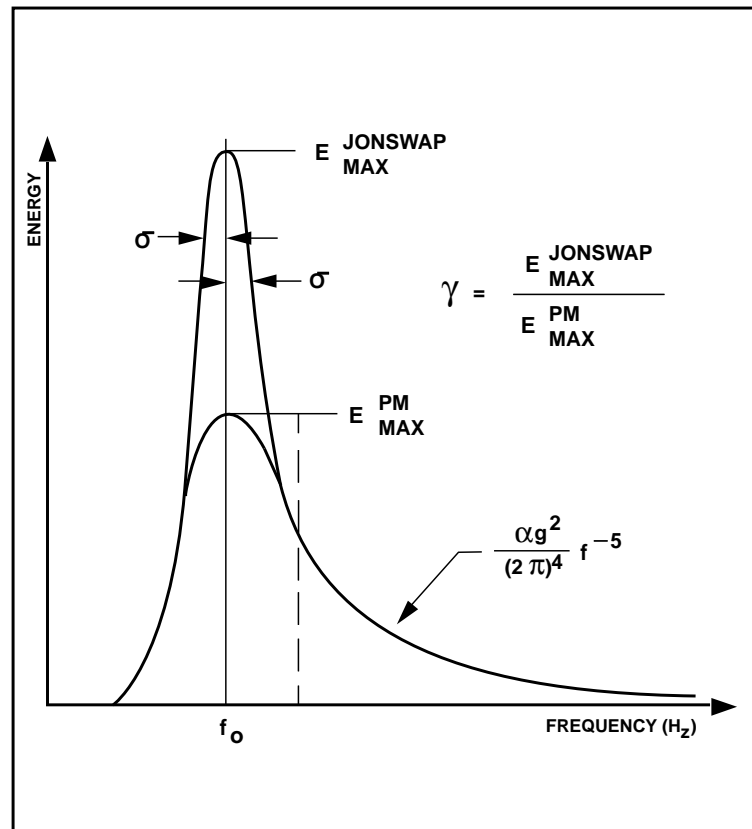with $\psi$ being a factor that incoporates the depth dependence.

Figure A.1: Comparison of the PM and JONSWAP spectra (Figure adapted from Hasselmann et al., 1973)

This spectrum accounts for shallow water effects such as wave-wave interaction, wave breaking and dissipation of wave energy due to the existence of a bottom boundary layer. The TMA spectrum may be interpreted as providing an upper bound on the energy at any particular frequency.

# Erklärung

Hiermit versichere ich, daß ich diese Arbeit selbstständig verfaßt und keine anderen als die angegeben Quellen und Hilfsmittel benutzt habe.

Alger Werft                                    Hamburg, den 24. Februar 2003